Northern Hemisphere Wintertime Teleconnections from the 2023-2024 El Niño Offset by Background SST Trends

Clara Deser*, Stephen Yeager, Adam S. Phillips, Nan Rosenbloom and Xueying Zhao

NSF National Center for Atmospheric Research, Boulder, CO, United States

Submitted to *J. Climate*

April 18, 2025

Revised August 18, 2025

* Corresponding author: Dr. Clara Deser, Climate and Global Dynamics Laboratory, NSF-NCAR, Boulder CO 80305; cdeser@ucar.edu.

Abstract

The El Niño of 2023-2024 ranked among the top 5 strongest El Niño events of the past 70 years, yet wintertime atmospheric teleconnections to the extra-tropical Northern Hemisphere were markedly weaker than anticipated. Here, we conduct a series of atmospheric modeling experiments using prescribed observed SSTs and radiative forcings to test the hypothesis that the observed pattern of background SST trends since 1980 was responsible for counteracting the expected teleconnection response. This so-called "SST pattern effect" (enhanced warming in the Tropical Indian and Atlantic Oceans and relative cooling in the eastern tropical Pacific) is shown to drive a teleconnection of the opposite sign *via* a Rossby wave response to anomalous precipitation over the western tropical Pacific driven remotely from the Indian Ocean. The circulation response to the 2023-2024 El Niño in the absence of background SST changes is almost entirely cancelled by the teleconnection produced by SST trends, with consequences for precipitation impacts over North America and Europe. Analogous behavior is found for the observed circulation anomalies, although internal atmospheric variability may also contribute. The results underscore the importance of considering the modulating influence of background SST trends, both natural and anthropogenic in origin, on El Niño teleconnections and associated climate impacts in the coming decades.

Significance statement

The El Niño of 2023-2024 ranked among the top 5 strongest El Niño events of the past 70 years, yet the expected wintertime atmospheric circulation and precipitation impacts over the Northern Hemisphere did not materialize. We investigate the reasons why this was the case and find that effects from long-term trends in tropical sea surface temperatures counteracted the expected El Niño teleconnections. Our results underscore the importance of considering the modulating influence of background sea surface temperatures on El Niño's fingerprint, especially as anthropogenic climate change accelerates in the coming decades.

1. Introduction

El Niño and La Niña events are naturally occurring phenomena that arise from coupled interactions between the ocean and atmosphere primarily within the tropical Pacific sector (e.g., Neelin et al. 1998; Chang et al. 2006; McPhaden et al. 2006; Wang et al. 2016). Strong El Niño events,

characterized by above normal sea surface temperatures (SSTs) in the eastern equatorial Pacific accompanied by slackened trade winds, typically last about one year and are followed by La Niña with anomalies of the opposite sign lasting for approximately two years (e.g., Harrison and Larkin, 1998; Okumura and Deser, 2010). This sequence recurs irregularly, roughly every 3-10 years, as part of the El Niño- Southern Oscillation (ENSO) cycle (Kessler 2002; Larkin and Harrison 2002; An et al. 2020). Strong ENSO events impact weather and climate worldwide through large-scale atmospheric and oceanic teleconnections to higher latitudes via Rossby wave dynamics and eddy-mean flow interactions (Bjerknes, 1969; Horel and Wallace, 1981; Ropelewski and Halpert, 1986; Trenberth et al. 1998; Held et al. 1989; Alexander et al. 2002). El Niño and La Niña events are now predictable at lead times of up to 6 and 18 months, respectively, providing an early-warning system of potential impacts (e.g., Lenssen et al. 2024; L'Heureux et al. 2020).

While the basic dynamics of ENSO events and their teleconnections are well understood, it is becoming increasingly clear that anthropogenic climate change can interfere with their evolution and impacts (e.g., Cai et al. 2021). In particular, global warming will act to enhance upper ocean stratification, which in turn can alter the strength and location of atmosphere-ocean coupling within the tropical Pacific, affecting the duration, amplitude and oscillatory nature of the ENSO cycle (Molina et al. 2025; Maher et al. 2023; Berner et al. 2020). Similarly, a warmer SST baseline will induce an eastward shift of the precipitation response to El Niño and La Niña SST anomalies, with implications for Rossby wave teleconnections (Zhou et al. 2014; Huang and Xie, 2015; Drouard and Cassou, 2019; Beverley et al. 2021). In addition, global warming will stabilize the tropical tropospheric temperature profile, reducing the sensitivity of tropical deep convection to SST departures relative to the tropical-mean SST (Sobel et al. 2001; Johnson and Xie, 2010; Johnson and Kosaka, 2016; Izumo et al. 2020). Besides potentially modifying the characteristics of ENSO itself, anthropogenic forcing will alter the mean state of the extra-tropical atmospheric circulation, including the strength and position of the subtropical and midlatitude jet streams (e.g., Barnes and Polvani, 2013; Simpson et al. 2014). These base state changes will impact Rossby wave source generation by tropical precipitation and associated upper-level divergent circulation anomalies, with downstream effects on Rossby wave teleconnections and eddy-mean flow interactions (Drouard and Cassou, 2019; Beverley et al. 2021 and 2024).

ENSO dynamics and teleconnections are also sensitive to mean-state changes associated with natural climate fluctuations, including glacial-to-interglacial cycles on millennial time scales and shorter-term variations associated with phenomena such as “Atlantic Multi-decadal Variability” (AMV) and “Pacific Decadal Variability” (PDV): Gershunov and Barnett, 1998; Timmermann et al. 2007; Capotondi et al. 2015; Maher et al. 2022; Thirumalai et al. 2024. However, the nature and dynamics of this sensitivity are not fully understood due to limited information from available observational and paleo-proxy archives and the presence of large inherent stochastic variability in both the ENSO cycle itself (Wittenberg, 2009; Deser et al. 2012) and the extratropical atmospheric circulation (Deser et al. 2017).

The El Niño of 2023-2024 occurred against a backdrop of natural climate variability and accelerating global warming, ranking among the top 5 strongest El Niño events of the past 70 years according to the Oceanic Niño Index (ONI; NOAA Climate Prediction Center, 2024). Contrary to expectation, however, the atmospheric teleconnection to the Northern Hemisphere (NH) extra tropics in boreal winter 2023-2024 was markedly weaker than anticipated based on historical precedent (Zhang et al. 2025), as were the climate impacts over the contiguous United States (L’Heureux et al. 2024). Analyses of upper-level geopotential height anomaly forecasts from the North American Multi-Model Ensemble (NMME) and Reanalysis products showed that global SST warming trends in recent decades contributed to the weaker-than-expected teleconnection pattern by elevating geopotential heights globally, thereby offsetting the El Niño–induced deepening of the Aleutian Low (Chen et al. 2024). Atmospheric modeling experiments further highlight the role of tropical Indian and Atlantic SSTs, which were exceptionally high during 2023-2024, in counteracting the expected El Niño teleconnection to the North Pacific (Zhang et al. 2025).

In this work, we build upon the aforementioned studies to probe the dynamical mechanisms underlying the role of background SST trends on NH teleconnections forced by the 2023-2024 El Niño during boreal winter December-February (DJF). As in those studies, we focus on the period since 1980 when SST trends show a distinctive spatial structure consisting of cooling in the eastern tropical Pacific and Southern Ocean and warming elsewhere (Wills et al. 2022). This SST trend pattern has received considerable attention in recent years, as it goes against model projections

which generally show enhanced warming in the equatorial eastern Pacific (e.g., an El Niño-like pattern) in response to anthropogenic climate change. The origin of the observed trend pattern is likely a combination of internal variability and anthropogenic forcing, although the relative contribution of each is under active debate (Wills et al. 2022; Heede and Federov, 2023; Watanabe et al. 2024). The distinctive spatial structure of the recent trend has been dubbed the "SST Pattern Effect" in recognition of its importance for cloud radiative feedbacks that control transient climate sensitivity (e.g., Dong et al. 2019, 2021; Rugenstein et al. 2023; Armour et al. 2024). Here, we elucidate its relevance for teleconnections and associated precipitation impacts over North America and Europe during the 2023-2024 El Niño. Our results are based on a series of AMIP experiments with Community Atmospheric Model version 6 (CAM6) at 1° spatial resolution, which shed light on the relative contributions and dynamical mechanisms of teleconnections forced by SST trends in the tropics *vs.* extra tropics and the tropical Pacific *vs.* tropical Indo-Atlantic. Our model results are compared with the observed circulation and precipitation anomalies during DJF 2023-2024, taking into account the role of internal atmospheric variability.

The rest of this study is organized as follows. Our data sets, model experiments and analysis procedures are described in Section 2. Results are presented in Section 3, and summarized and discussed in Section 4.

2. Data and Methods

a. Observations and Reanalysis Data

We use the following data sets covering the period 1979-2024 at monthly resolution:

1) Terrestrial precipitation from the Global Precipitation Climatology Centre (GPCC) dataset on a 1°x1° grid (Schneider et al., 2014);
2) Global precipitation from the Global Precipitation Climatology Product (GPCP) v2.3 on a 2.5°x2.5° grid (Adler et al. 2018);
3) Sea surface temperature from the National Oceanic and Atmospheric Administration (NOAA) ERSSTv5 dataset on a 2°x2° grid (Huang et al. 2017);
4) Sea ice concentration from the National Snow and Ice Data Center version 4 on a 25km x 25km grid (DiGirolamo et al. 2022).

5) Sea level pressure (SLP), 500hPa geopotential height (Z500), and 250hPa zonal and meridional wind (U250, V250) from the ECMWF Reanalysis v5 (ERA5) on a 1°x1° grid (Hersbach et al. 2020).

b. Modeling Experiments

We use CAM6 coupled to Community Land Model version 5 (CLM5) at a nominal spatial resolution of 1°. CAM6 and CLM5 are the atmospheric and terrestrial model components of Community Earth System model version 2 (CESM2; Danabasoglu et al. 2020). CAM6 has substantially improved representation of the large-scale atmospheric circulation compared to its predecessor CAM5, ranking within the top 10% of CMIP6-class atmospheric models in many respects (Simpson et al. 2020). In particular, CAM6 simulates with good fidelity the global divergent circulation and the boreal winter Northern Hemisphere (NH) jet streams, storm tracks, stationary waves, blocking and modes of variability such as the Northern Annular Mode and the North Atlantic Oscillation (Simpson et al. 2020).

We conduct a parsimonious set of AMIP experiments with CAM6/CLM5 aimed at understanding the dynamical mechanisms underlying the global atmospheric circulation response to observed SST and sea ice concentration (SIC) anomalies in DJF 2023-2024; salient details of each experiment are given in Table 1. All experiments consist of 50 ensemble members beginning on November 1 and ending on April 30. Initial conditions are derived following the methodology used in the CESM2 Seasonal-to-multiyear Large Ensemble (SMYLE) prediction system (Yeager et al., 2022). Specifically, CAM6 is initialized by interpolating Japanese 55-year atmospheric reanalysis (JRA55; Kobayashi et al., 2015) fields from November 1, 2023; CLM5 initial conditions are obtained from a forced land-only simulation driven by JRA55. Ensemble spread is created by randomly perturbing the initial atmospheric temperatures by a small amount (order 10^{-14}K). The lower boundary conditions for all experiments utilize SST from ERSSTv5 (Huang et al. 2017) and SIC from NSIDC CDR (DiGirolamo et al. 2022). To derive perturbed SST/SIC boundary conditions for the experiments, climatological monthly means are computed over the period 1979-2024 and monthly anomalies are formed by subtracting the climatology for each month separately.

We isolate the impact of changes in background SST/SIC trends by constructing a counterfactual version of the observed 2023-2024 SST/SIC anomalies from which the linear trend (computed for each month separately over the period 1979-2024) per 45 years has been subtracted (the December, January and February trend maps are all very similar; not shown). The Counterfactual can be thought of as the SST/SIC anomalies that would have occurred in a 1979-1980 background state, all other factors being equal. We emphasize that the evolution of the 2023-2024 El Niño event itself was likely modulated by background SST trends (Peng et al. 2025) in addition to inter-basin processes operating on interannual time scales (e.g., Cai et al. 2019; Wang 2019; Kim et al. 2025; Zhang et al. 2025). Thus, our counterfactual version is not intended to represent what the El Niño would have looked like in the absence of background SST trends and interannual inter-basin influences; rather, we use it to isolate the impact of background SST trends on atmospheric teleconnections driven by the actual 2023-2024 SST anomalies.

We conduct AMIP experiments with both the actual and Counterfactual 2023-2024 SST/SIC anomalies added to the monthly SST/SIC climatology. Contemporaneous monthly radiative forcings are used for these experiments (e.g., corresponding to 2023-2024 and 1979-1980 for the actual and Counterfactual, respectively, except for volcanoes which are kept at 2023-2024 conditions to avoid any issues related to changing background aerosols). These paired AMIP experiments are configured for four regional domains: global, tropical, tropical Pacific and tropical Indo-Atlantic (boundaries of each regional domain are given in Table 1). For the regional experiments, monthly SST/SIC anomalies outside of the domain are linearly tapered to zero within a 7° latitude and 7° longitude buffer zone, and a monthly climatology is used outside of the buffer zone. We shall refer to these experiments as: “Global”, “Tropical”, “TropPac” and “TropIndAtl”, followed by either “2023-24” or “Counterfactual”; a square bracket is used to denote the 50-member ensemble-mean. We also perform a paired set of 50-member control AMIP experiments (CTL2024 and CTL1980) using monthly climatological SST/SIC everywhere (no anomalies). Monthly radiative forcings corresponding to 2023-2024 and 1979-1980 (except for volcanoes as described above) are used for CTL2024 and CTL1980, respectively. All results are based on DJF averages.

We assess the response to changes in radiative forcing in the absence of changes in SST and SIC from [CTL2024] – [CTL1980]. Similarly, we obtain the response to the Counterfactual SST/SIC anomalies by subtracting [CTL1980] from the ensemble-mean of each Counterfactual experiment. The response to the actual 2023-2024 SIC/SST anomalies in combination with radiative forcing changes is found by subtracting [CTL1980] from the ensemble-mean of each 2023-24 experiment. Finally, differencing the paired ensemble-mean 2023-24 and Counterfactual experiments yields the response to SST/SIC trends in combination with radiative forcing changes: for example, [Global 2023-24] – [Global Counterfactual]. We assess statistical significance of the forced responses by applying a 2-tailed Student's-t test at the 5% confidence level to the difference between the two 50-member distributions.

Table 1. AMIP Experimental design (see text for details).

Experiment Name	**SST/SIC anomaly domain**	**2023-24** (2023-24 Radiative Forcing)	**Counterfactual** (1979-80 Radiative Forcing)
Global	90°N-90°S, 0°-360°E	x	x
Tropical	28°N-28°S, 0°-360°E	x	x
TropPac	28°N-28°S, 112°-285°E	x	x
TropIndAtl	28°N-28°S, 68°W-105°E	x	x
CTL	N/A	x	x

c. Rossby Wave Source and Wave Activity Flux

We compute the 250 hPa Rossby Wave Source (RWS) following Sardeshmukh and Hoskins (1988) and the 250 hPa Rossby Wave Activity Flux (WAF) following Takaya and Nakamura (2001). The RWS is derived from the barotropic vorticity equation and includes a vortex stretching term that represents the effect of divergence on vorticity changes, and a vorticity advection term that represents the effect of absolute vorticity advection by the divergent flow. The WAF provides a metric of wave propagation parallel to the local group velocity of stationary Rossby Waves. Details and mathematical derivations may be found in the papers cited above.

3. Results

a. Observed SST anomaly patterns

In DJF 2023-24, SSTs were well above the long-term (1979-2024) climatology across the entire equatorial Pacific Ocean, with maximum anomalies around 2°C near 170°W and 110°W (Fig. 1a). Large positive SST anomalies were also found over the western half of the northern Indian Ocean and off-equatorial portions of the tropical Atlantic Ocean, with peak values around 1.5°C rivaling those in the equatorial Pacific. At higher latitudes, SSTs were well above normal over the northwest Pacific Ocean east of Japan and over the Labrador Sea, and slightly below normal over the subtropical southeast Pacific and parts of the Southern Ocean. SIC anomalies are generally consistent with adjacent SST anomalies (e.g., negative SST anomalies within the marginal ice zones correspond to positive SIC anomalies and vice versa; Fig. A1a).

The Counterfactual SST anomalies featured a more canonical El Niño pattern, with values reaching nearly 2.8°C in the central equatorial Pacific, surrounded by a horse-shoe shaped pattern of moderate cooling in the far western tropical Pacific extending into the subtropics of both hemispheres (Fig. 1b). Counterfactual SST anomalies in the tropical Atlantic and Indian Oceans were also positive, but considerably weaker than those in the equatorial Pacific. Unlike the actual 2023-2024 SST anomalies, the Counterfactual anomalies display only minor warming east of Japan and pronounced cooling in the North Atlantic. Counterfactual SICs were above normal throughout the Arctic marginal ice zones, consistent with the cooler SSTs, and slightly below (above) normal along east (west) Antarctica in keeping with the local SSTs (Fig. A1b).

The SST trends display a negative PDV-like pattern, with cooling over the southeast subtropical Pacific extending onto the equator in the central Pacific, surrounded by warming maxima in the western tropical Pacific and the midlatitude north and south Pacific; relatively amorphous warming is found throughout the tropical Indian and Atlantic Oceans (Fig. 1c). At higher latitudes, cooling is seen over much of the Southern Ocean, while warming occurs over the western North Atlantic and the subpolar seas north of Iceland and Scandinavia, accompanied by diminished SIC (Fig. S1c). Notably, the SST trends and Counterfactual SST anomalies show generally similar large-scale patterns but their polarity is opposite, which suggests that they may have counteracting influences on global atmospheric teleconnections.

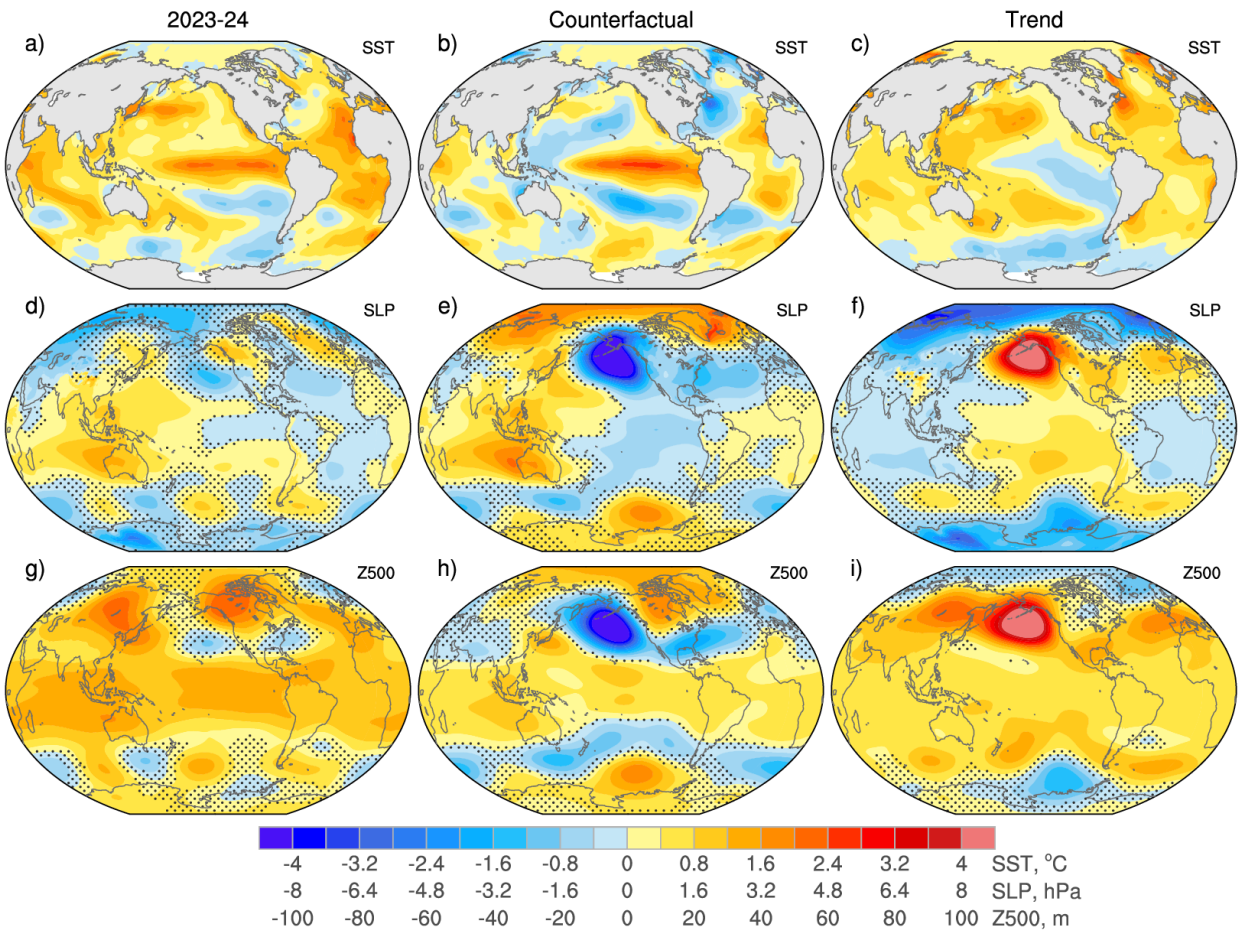

Figure 1. (Top row) Observed DJF SST anomalies: a) 2023-24; b) Counterfactual; c) Trend. (Middle and bottom rows) CAM6 DJF SLP (hPa) and Z500 (m) responses to Global SST/SIC anomalies: d,g) [Global 2023-24] – [CTL1980]; e,h) [Global Counterfactual] – [CTL1980]; f,i) [Global 2023-24] – [Global Counterfactual]. Responses without stippling are statistically significant at the 5% confidence level.

b. Atmospheric circulation and precipitation responses

Figure 1 (lower panels) compares the CAM6 DJF SLP and Z500 responses to Global 2023-2024, Global Counterfactual and Global Trend SST/SIC anomalies, defined as [Global 2023-24] – [CTL1980], [Global Counterfactual] – [CTL1980], and [Global 2023-24] - [Global Counterfactual], respectively. The relatively weak circulation response to Global 2023-2024 SST/SIC anomalies is due to the large cancellation between the Counterfactual and Trend responses, especially over the NH extra-tropics (Figs. 1e,f and h,i). In particular, the

Counterfactual SST/SIC anomalies drive a pronounced deepening of the Aleutian Low (maximum amplitude of ~11 hPa in SLP and 130m in Z500) while the Trend drives the opposite-signed response of nearly equal magnitude (maximum value ~10 hPa in SLP and 140m in Z500). Similarly, the Counterfactual produces a negative North Atlantic Oscillation (NAO) response in both SLP and Z500 that is largely counteracted by the positive NAO response to the Trend. Offsetting effects are also apparent in the extratropical Southern Hemisphere (SH) circulation responses. Within the tropics, the SLP responses are of opposite sign, indicative of a negative (positive) Southern Oscillation response to the Counterfactual (Trend) SST/SIC anomalies; however, the Z500 responses are of the same sign, with a zonally homogenous pattern of positive anomalies (magnitudes ~10-20m) throughout the tropical belt.

Because of the opposing effects of the Global Counterfactual and Global Trend responses, the extra-tropical teleconnections driven by the 2023-2024 SST/SIC anomalies are relatively weak and spatially disorganized (Figs. 1d,g). In particular, the expected deepening of the Aleutian Low is only apparent over a limited portion of the North Pacific, with maximum amplitude ~2.5 hPa in SLP and ~ 20m in Z500, and the NAO response is largely absent. In the tropics, the expected negative Southern Oscillation SLP response is relatively muted, especially in the eastern equatorial Pacific; however, the tropical Z500 response is nearly doubled in amplitude compared to the Counterfactual El Niño due to the constructive contribution from the Trend response.

The Trend response contains impacts from both radiative and SST changes. To separate these two effects, we subtract the two control simulations ([CTL2024] minus [CTL1980]) to obtain the radiatively-forced contribution; we then subtract the radiative contribution from the Trend response to derive the SST/SIC-forced contribution. SST/SIC forcing dominates the overall Trend response, as evidenced by the similarity in pattern and amplitude of the circulation anomalies (Fig. 2b,c and e,f). In particular, the spatial correlation between the Trend and SST/SIC-forced responses is 0.91 for SLP and 0.92 for Z500, and the spatial root-mean-squared (rms) difference (as a fraction of the spatial rms of the trend response) is 0.42 for SLP and 0.29 for Z500. Radiative forcing makes only a minor contribution to the overall trend response, with much weaker pattern correlations and greater rms differences (0.53 for SLP and 0.40 for Z500, and 0.86 for SLP and 0.89 for Z500, respectively; Fig. 2a,c and d,f). The radiatively forced response projects onto the

positive phase of the Northern and Southern Annular Modes in the extra tropics, and contributes to an out-of-phase SLP response between the tropical Atlantic and tropical Indo-Pacific, and a zonally-uniform increase in Z500 over the tropical belt (Figs. 2a,d).

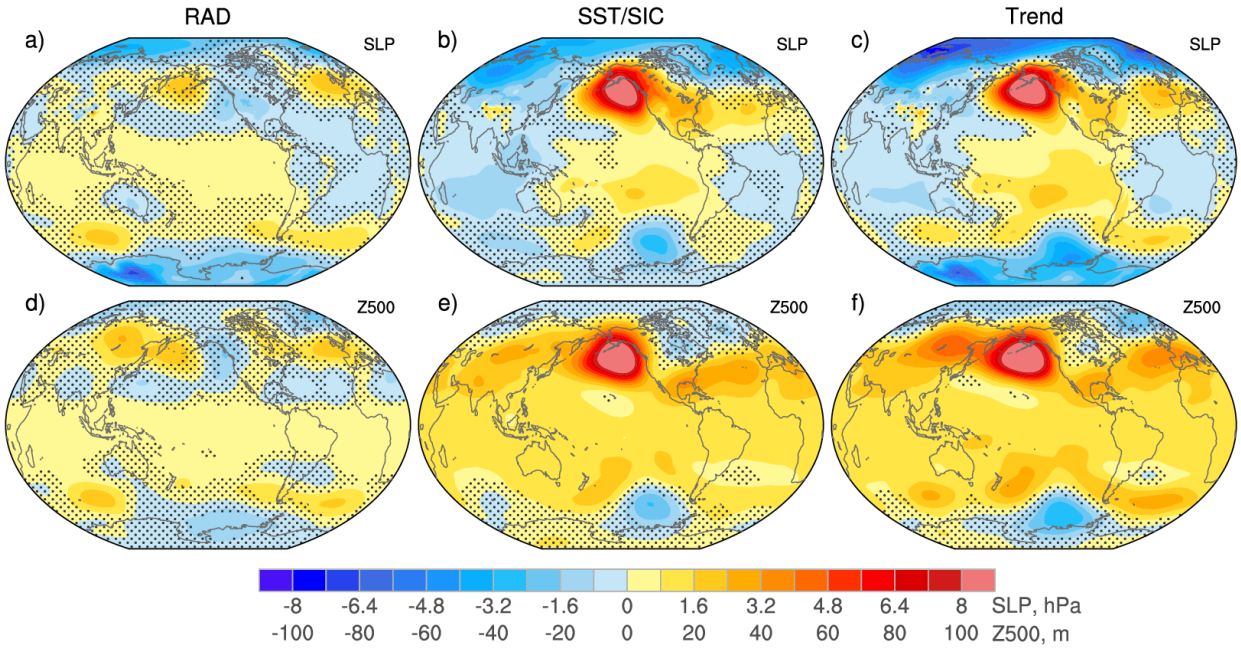

Figure 2. Decomposition of the CAM6 DJF (top) SLP (hPa) and (bottom) Z500 (m) Trend responses into radiative and SST/SIC forced components. (a,d) Radiatively-forced (RAD); (b,e) SST/SIC-forced; (c,f) Trend response [Global 2023-24] – [Global Counterfactual]. See text for details. Responses without stippling are statistically significant at the 5% confidence level.

The opposing circulation responses over the NH extra tropics to the Counterfactual El Niño and Trend components of the 2023-2024 SST anomalies have important consequences for precipitation over North America and Europe (Fig. 3 and 4). Over North America, the Counterfactual El Niño produces wetter-than-normal conditions over much of the southern US and along the coasts of Alaska and British Columbia, and drier conditions over the Pacific Northwest extending into Idaho and the Dakotas, parts of western Canada-Alaska and the Ohio Valley – Upper South (Fig. 3b). The Trend generally causes opposite-signed impacts except over the Pacific Northwest where it augments the Counterfactual-induced drying (Fig. 3c). The relative balance of the two influences depends on the region. For example, the Counterfactual El Niño precipitation response dominates in the southeastern US, Ohio Valley – Upper South, Texas and New Mexico, while the Trend

dominates in Alaska and coastal British Columbia (Fig. 3a). In other areas, notably California, the northern Great Plains and Canadian Prairies, the two effects cancel almost completely (Fig. 3a).

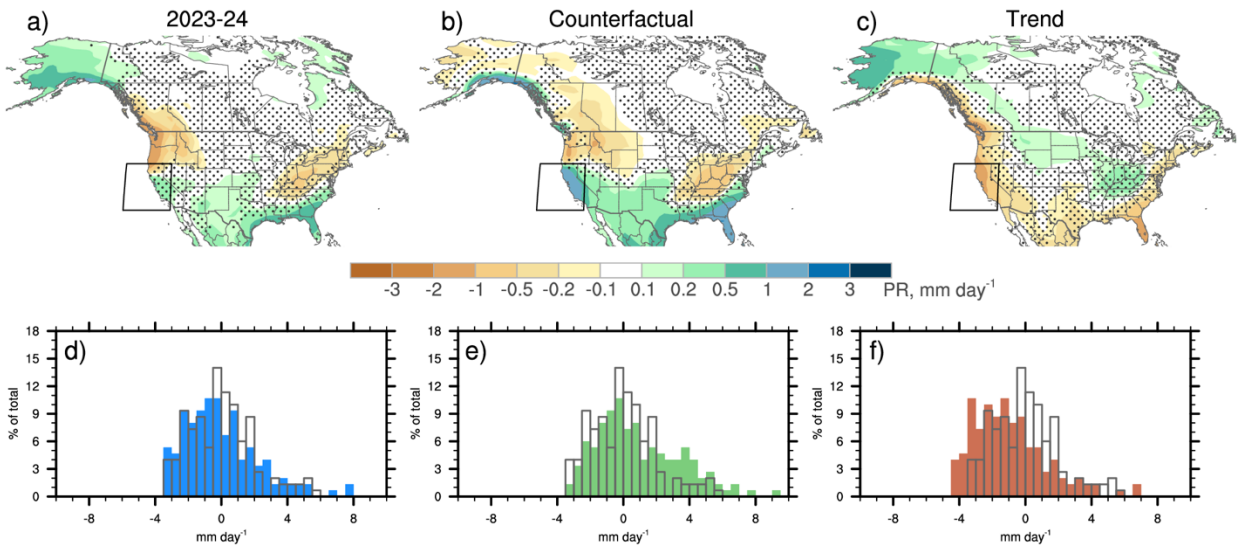

Figure 3. CAM6 DJF precipitation responses (mm day^{-1}) over North America to Global SST/SIC anomalies: a) [Global 2023-24] – [CTL1980]; b) [Global Counterfactual] – [CTL1980]; c) [Global 2023-24] – [Global Counterfactual]. Responses without stippling are statistically significant at the 5% confidence level. (d,e,f) Histograms of CAM6 DJF precipitation responses (mm day^{-1}) averaged over California (region outlined by the boxes in a-c): d) Individual members of Global 2023-2024 minus [CTL1980] in blue; e) Individual members of Global Counterfactual minus [CTL1980] in green; f) Individual members of Global 2023-2024 minus [Global Counterfactual] minus [CTL80] in brown. Open gray bars in d-f) show individual members of CTL1980 minus [CTL1980].

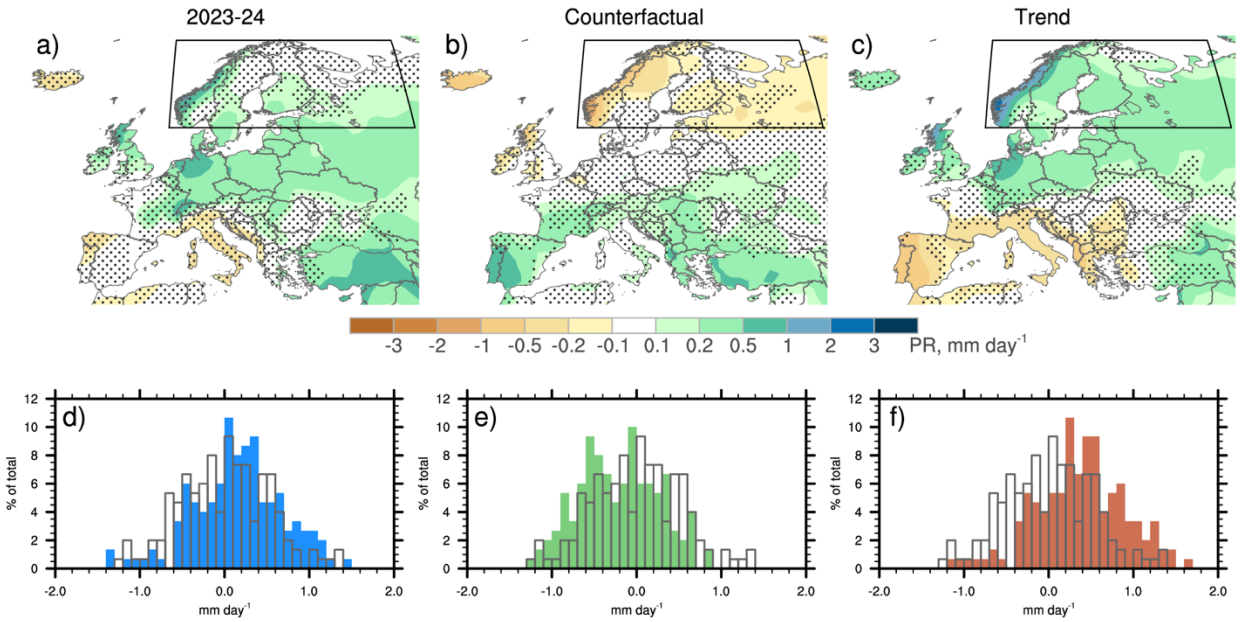

Figure 4. (a-c) As in Fig. 3a-c but for Europe. (d-f) As in Fig. 3d-f but for averages over northern Europe (region outlined by the boxes in a-c).

Histograms for California precipitation highlight the offsetting effects of the Counterfactual El Niño and Trend responses (Fig. 3d-f). Compared to the Control distribution (CTL1980), precipitation is preferentially increased in the (long) upper tail of the distribution in response to the Counterfactual El Niño and preferentially decreased in the (short) lower tail in response to the SST/SIC Trend, resulting in a nearly complete overlap between the CTL1980 and Global 2023-2024 distributions. In addition to the positive skewness, a notable aspect of the California precipitation distributions is the large range of values across ensemble members (spanning from approximately -4 mm day^{-1} to +8 mm day^{-1}), indicative of the contribution of internal atmospheric variability in any given winter.

Over Europe, the opposite-signed NAO responses to the Counterfactual El Niño and SST/SIC trend yield contrasting precipitation impacts, particularly over northern and southern portions of the continent (Fig. 4b,c) and extending eastward across much of Asia (Fig. A2b,c). For example, the negative NAO response to the Counterfactual El Niño causes drier conditions over the northern UK, Scandinavia and northwestern Russia, and wetter conditions over Portugal, Spain, southern France, the Balkans, Greece and Turkey, while the positive NAO response to the SST/SIC trend

drives generally opposite-signed precipitation impacts in these areas (except Turkey). As a result of the canceling effects, precipitation impacts from the 2023-2024 SST/SIC anomalies are mostly insignificant over northern and southern Europe. In contrast, precipitation over central Europe is predominantly influenced by the SST/SIC trend, which drives wetter than normal conditions, without any appreciable offset from the Counterfactual El Niño. This asymmetry is consistent with the eastward shift of the NAO response to the Trend compared to the Counterfactual (recall Figs. 1e,f and h,i), which in turn is partly a result of radiative forcing (Figs. 2a,d). Thus, the net effect of the anomalous forcing in 2023-2024 is to significantly enhance precipitation over central Europe and Turkey.

Precipitation histograms for northern Europe highlight the offsetting effects of the Counterfactual El Niño and Trend responses (Fig. 4k-l). The Counterfactual (Trend) distribution is significantly shifted toward drier (wetter) conditions compared to the Control distribution, and there is almost complete overlap between the CTL1980 and Global 2023-2024 distributions. Compared to California, the precipitation distributions for northern Europe are more gaussian in nature and show a smaller range across ensemble members (from approximately -1.4 mm day^{-1} to +1.4 mm day^{-1}).

c. Role of tropical vs. extra tropical SST anomalies

As a first step in gaining insight to the dynamical mechanisms underpinning the atmospheric circulation responses shown above, we isolate the contributions from SST anomalies in the tropics *vs.* SST/SIC anomalies in the extra tropics. The circulation responses to tropical SST anomalies (Fig. 5) are very similar to those induced by global SST anomalies (Fig. 1) for each of the experiments (2023-2024, Counterfactual and Trend), as evidenced by the high pattern correlations (0.88, 0.97 and 0.91 for SLP and 0.87, 0.97 and 0.83 for Z500) and relatively low rms differences (expressed as a fraction of the spatial rms of the response to global SST/SIC anomalies: 0.51, 0.24 and 0.41 for SLP and 0.32, 0.23 and 0.44 for Z500), respectively. Some small differences are found over the northern North Pacific and North Atlantic, mainly for the 2023-2024 and Trend responses, indicative of the influence of extra tropical SST anomalies.

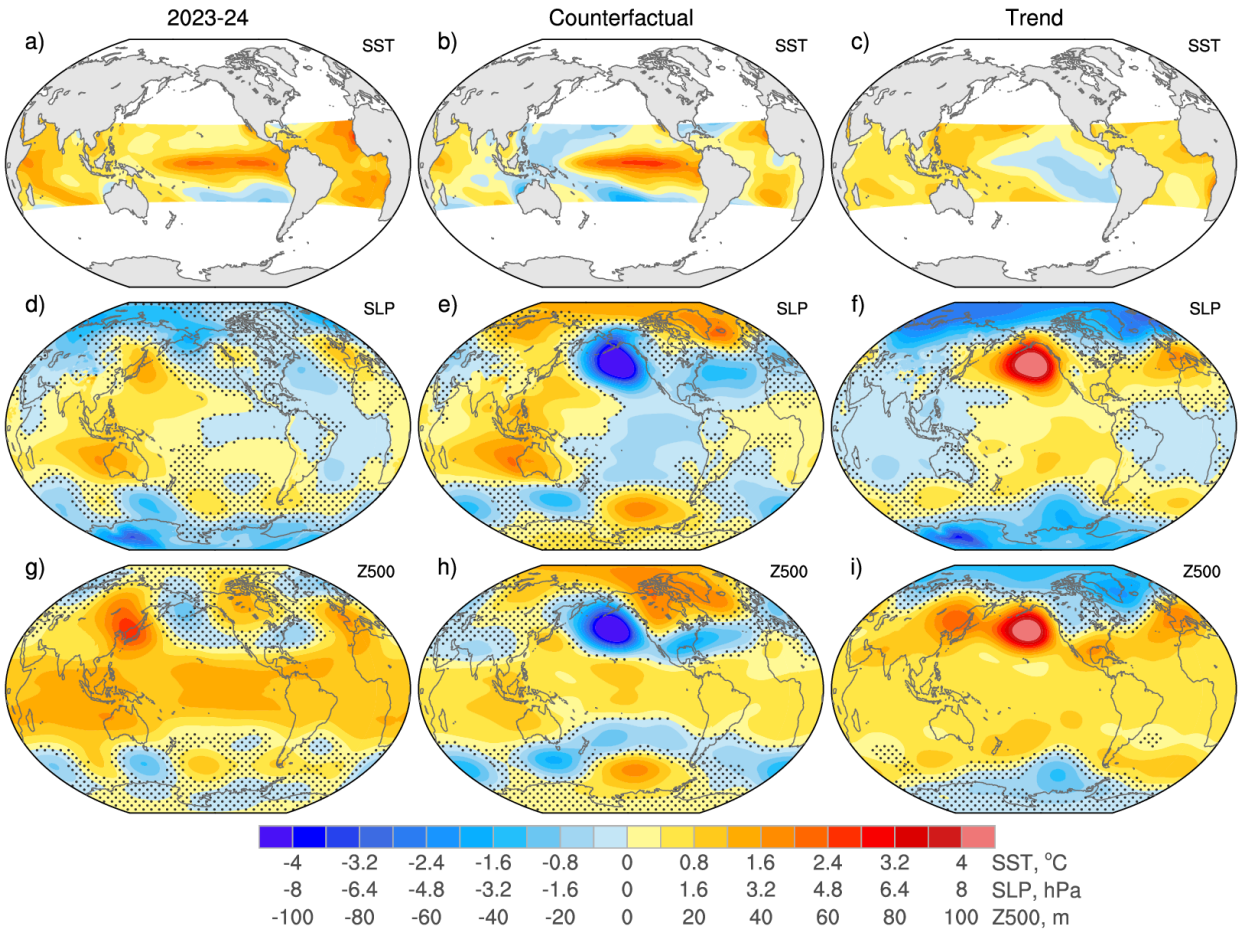

Figure 5. (Top row) Observed DJF tropical SST anomalies: a) 2023-24; b) Counterfactual; c) Trend. (Middle and bottom rows) CAM6 DJF SLP (hPa) and Z500 (m) responses to Tropical SST anomalies: d,g) [Tropical 2023-24] – [CTL1980]; e,h) [Tropical Counterfactual] – [CTL1980]; f,i) [Tropical 2023-24] – [Tropical Counterfactual]. Responses without stippling are statistically significant at the 5% confidence level.

The role of extra tropical SST anomalies is assessed by subtracting the Global and Tropical AMIP experiments. The SST warming trend along the Kuroshio Extension appears to drive a local reduction in SLP and Z500 coupled with an increase over Alaska and the Bering Sea (Fig. 6 f,i). These responses are modest in amplitude (up to ~3 hPa and ~40 m), but nonetheless statistically significant due to the large ensemble size of the experiments. A weak but statistically significant Z500 increase is also found over the Labrador Sea and western subpolar north Atlantic, likely in response to the local SST warming trend. Both features are apparent in the response to the 2023-2024 SST anomalies, but with diminished amplitude due to partially offsetting effects from the Counterfactual (Figs. a,d,g). The only statistically significant circulation response to extra tropical

SST anomalies in the Counterfactual case is the small decrease in SLP and Z500 over the Bering Sea (extending into Alaska for SLP), likely in response to local SST cooling, and a patch of weak negative Z500 anomalies over the western tropical Pacific (Figs. 6 e,h). We note that our AMIP experiments cannot address the origin of the extra tropical SST anomalies (e.g., to what extent they may be driven by the atmospheric circulation); they can only reveal how the extra tropical SST anomalies feedback upon the atmosphere.

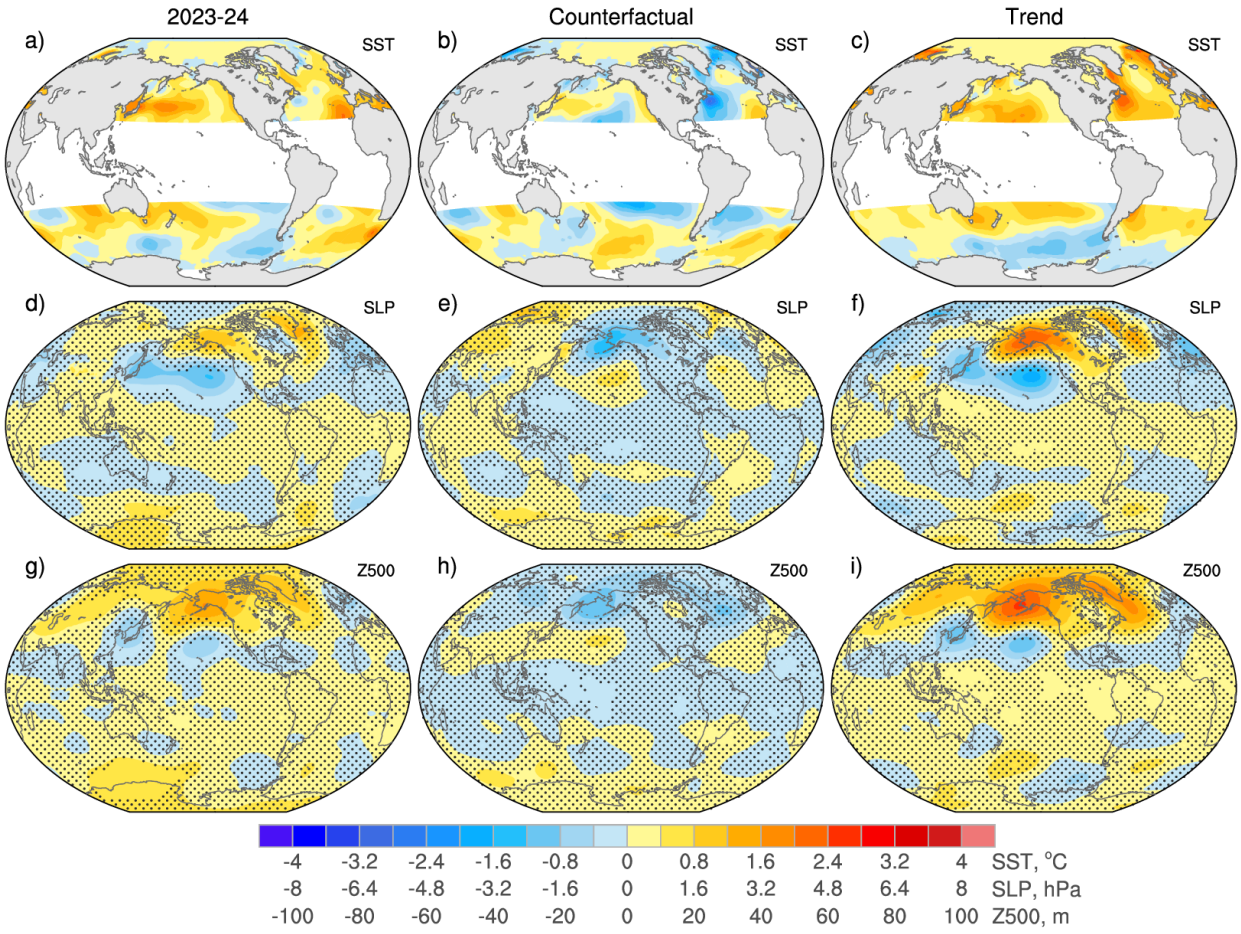

Figure 6. As in Fig. 5 but for the difference between the Global and Tropical AMIP experiments. (Top row) Observed DJF extra tropical SST anomalies: a) 2023-24; b) Counterfactual; c) Trend. (Middle and bottom rows) Inferred CAM6 DJF SLP (hPa) and Z500 (m) responses to extra tropical SST anomalies: d,g) ([Global 2023-24] – [CTL1980]) minus ([Tropical 2023-24] – [CTL1980]); e,h); ([Global Counterfactual] – [CTL1980]) minus ([Tropical Counterfactual] – [CTL1980]); f,i) d)-e) and g)-h). Responses without stippling are statistically significant at the 5% confidence level.

d. Role of tropical Pacific vs. Indo-Atlantic SSTs

The results shown above highlight the role of the tropics in driving the counteracting circulation responses to the Counterfactual and Trend components of the 2023-2024 SST anomalies. Here, we investigate the relative contributions of SST anomalies in the tropical Pacific *vs.* tropical Indo-Atlantic. Tropical Indo-Atlantic SST trends drive strong positive SLP and Z500 responses over the North Pacific and (with weaker amplitude) eastern North Atlantic, and negative responses over the Arctic (Figs. 7c,f), while tropical Pacific Counterfactual SST anomalies produce a marked deepening of the Aleutian Low and a negative NAO (Figs. 7h,k). The responses to Tropical Indo-Atlantic Counterfactual SST anomalies and Tropical Pacific SST trends are considerably weaker than their Trend and Counterfactual counterparts, respectively (Figs. 7b,e and i,l). Thus, it is the combination of tropical Indo-Atlantic SST trends and tropical Pacific Counterfactual SST anomalies that is primarily responsible for the weaker-than-expected teleconnections to the NH extra tropics during DJF 2023-2024. Qualitatively similar results are found when the response to tropical Indo-Atlantic SST trends (tropical Pacific Counterfactual SST anomalies) is inferred from the difference between the pan-tropical and tropical Pacific (tropical Indo-Atlantic) experiments, albeit with some differences in magnitude indicative of non-linear inter-basin interactions (not shown).

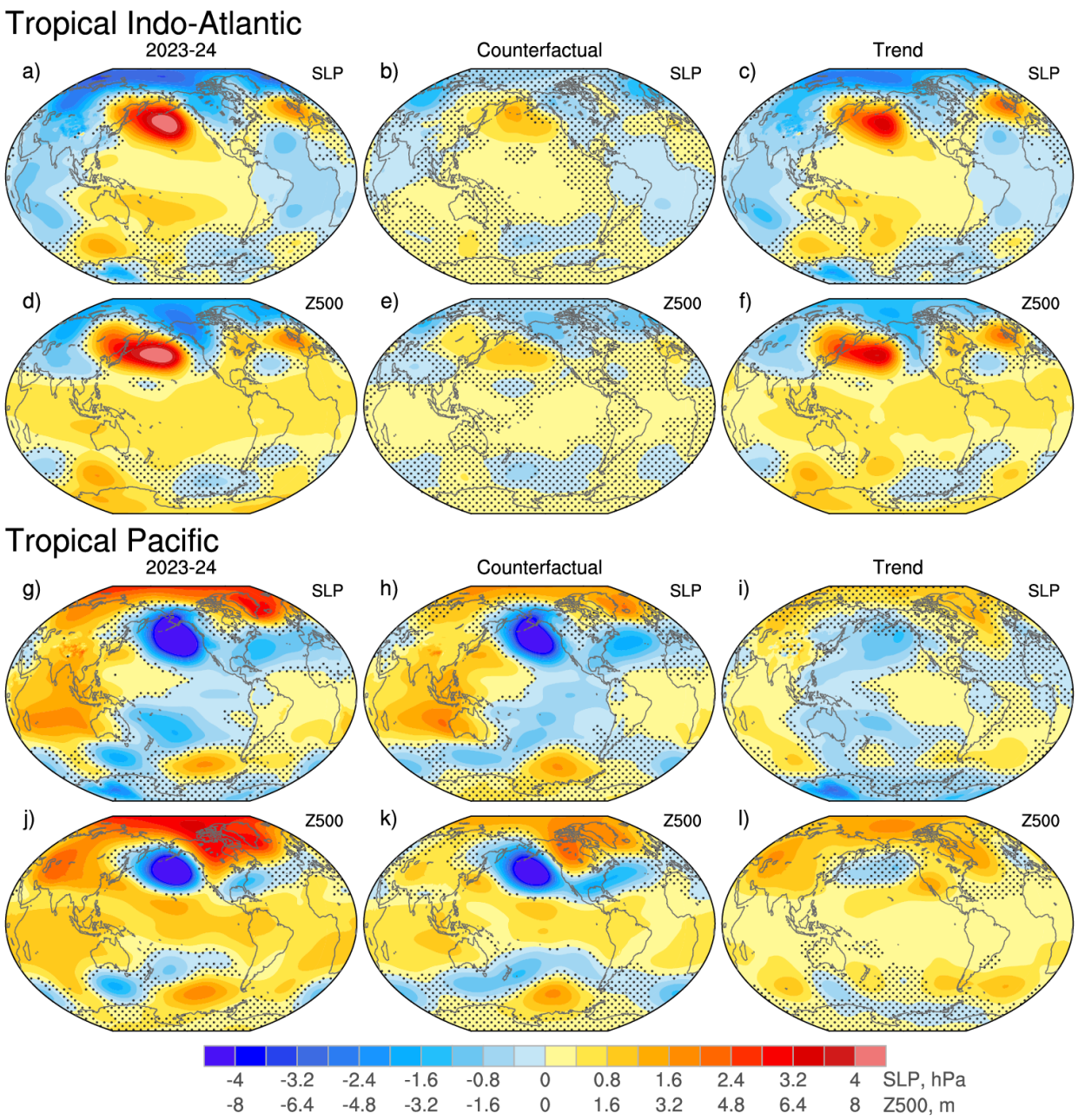

Figure 7. CAM6 DJF (a-c) SLP (hPa) and (d-f) Z500 (m) responses to Tropical Indo-Atlantic SST anomalies: a,d) [TropIndAtl 2023-24] – [CTL1980]; b,e) [TropIndAtl Counterfactual] – [CTL1980]; c,f) [TropIndAtl 2023-24] – [TropIndAtl Counterfactual]. (g-l) As in (a-f) but for the response to Tropical Pacific SST anomalies: g,j) [TropPac 2023-24] – [CTL1980]; h,k) [TropPac Counterfactual] – [CTL1980]; i,l) [TropPac 2023-24] – [TropPac Counterfactual]. Unstippled areas are statistically significant at the 5% confidence level.

e. Teleconnection dynamics

What are the dynamical mechanisms governing the circulation responses to the Counterfactual and Trend components of the 2023-2024 SST anomalies in the tropical Indo-Atlantic and Pacific? We begin by showing the precipitation and 250 hPa meridional wind (V250) responses for an overall view of the teleconnection dynamics, followed by a more detailed examination based on RWS and WAF diagnostics.

The precipitation response to 2023-2024 SST anomalies in the tropical Indo-Atlantic consists of local and non-local features (Fig. 8a). Locally over the Indian Ocean, precipitation increases over the western side of the basin and along ~5°N, and decreases along the equator, consistent with the pattern of SST anomalies (recall Fig. 5a). Local precipitation increases are also found along ~5°N in the Atlantic, but they are considerably weaker than those in the Indian Ocean. Colder mean state SSTs and smaller SST anomaly gradients in the tropical Atlantic compared to the tropical Indian Ocean may contribute to the weaker precipitation response. A strong non-local precipitation response is found over the western tropical Pacific, with drying on both sides of the equator and wetting in between; the amplitude of the non-local drying rivals (and even exceeds) the local wetting over the western Indian Ocean. The non-local precipitation response over the western tropical Pacific is driven by an anomalous zonal circulation cell, with upward motion over the Indian Ocean associated with locally enhanced precipitation and downward motion over the western tropical Pacific (not shown), which acts to inhibit precipitation in areas of maximum climatological rainfall (Fig. S2a). Such a non-local precipitation response is consistent with results from idealized atmospheric modeling experiments with imposed Indian Ocean SST warming (e.g., Hurrell et al. 2004; Hoerling et al. 2004; Deser and Phillips, 2006).

In contrast to 2023-2024, the precipitation response to the Counterfactual El Niño SST anomalies in the tropical Indo-Atlantic sector is primarily local, with largest amplitudes over the Indian Ocean featuring a meridional dipole pattern similar to that of 2023-2024 (Fig. 8b). The precipitation response to tropical Indo-Atlantic SST trends shows a strong non-local response over the western tropical Pacific similar to that of 2023-2024, along with weaker local responses over the Indian and Atlantic sectors (Fig. 8c).

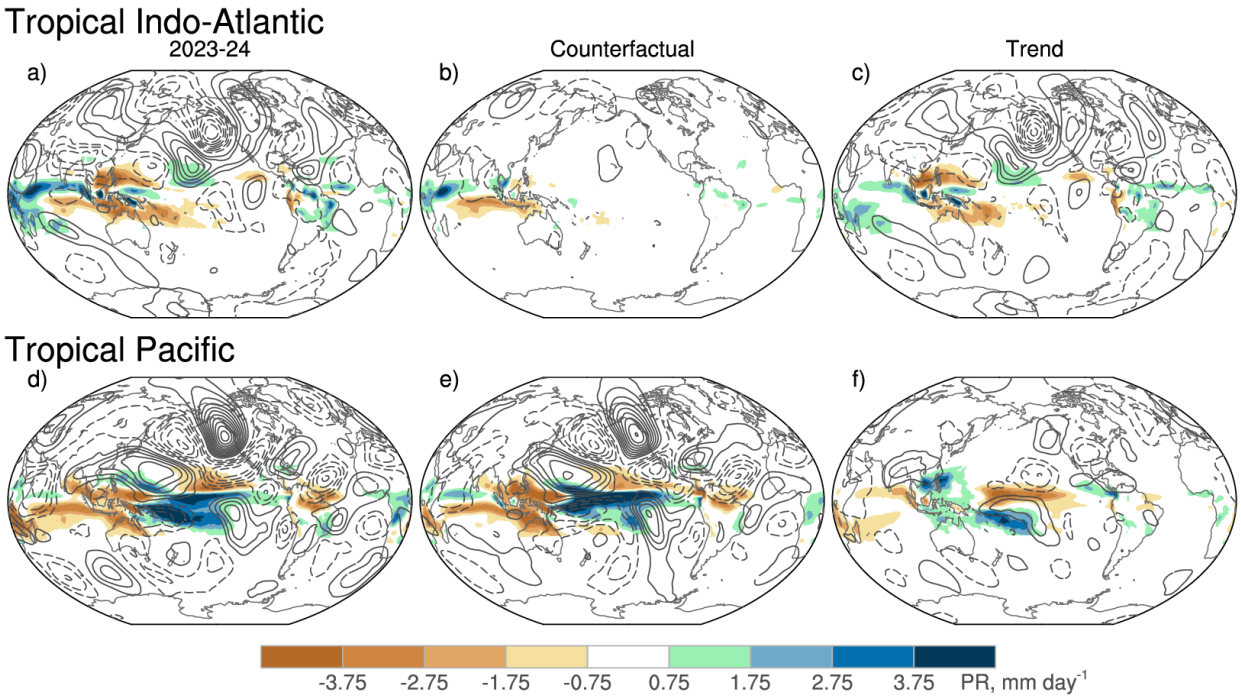

Figure 8. CAM6 DJF precipitation (color shading; mm d^{-1}) and V250 (contour interval of 1 ms^{-1}; solid contours for positive values and dashed contours for negative values) responses to (a-c) Tropical Indo-Atlantic and (d-f) Tropical Pacific SST anomalies. a) [TropIndAtl 2023-24] – [CTL1980]; b) [TropIndAtl Counterfactual] – [CTL1980]; c) [TropIndAtl 2023-24] – [TropIndAtl Counterfactual]; d) [TropPac 2023-24] – [CTL1980]; e) [TropPac Counterfactual] – [CTL1980]; f) [TropPac 2023-24] – [TropPac Counterfactual]. For clarity, only precipitation responses within the tropics (25°N-25°S) are shown.

The V250 response to tropical Indo-Atlantic SST trends exhibits two arcing NH wave trains that emanate from the *non-local* precipitation response (drying) in the far western tropical Pacific (Fig. 8c). One wave train originates over the Tibetan Plateau and southeastern China and the other originates near 20°N, 160°E. The former takes a more poleward route over eastern Asia, the Arctic and northern Canada, while the latter propagates into the Gulf of Alaska and turns southeastward across North America and into the far western tropical Atlantic. Similar V250 wave train responses are found for the 2023-2024 tropical Indo-Atlantic SST anomalies, with enhanced amplitudes on the western side of the Asian wave train (Fig. 8a). The tropical Indo-Atlantic component of the Counterfactual SST anomalies shows a very weak V250 response (Fig. 8b). These results underscore the importance of the non-local precipitation response in the western tropical Pacific

to tropical Indo-Atlantic SST trends, which triggers a NH teleconnection of opposite sign to that induced by the Counterfactual El Niño via tropical Pacific SSTs.

The 2023-2024 and Counterfactual SST anomalies in the tropical Pacific cause an increase in precipitation over the central equatorial Pacific and a reduction to the west, extending over the Maritime Continent and equatorial Indian Ocean (Figs. 8d,e). The positive precipitation anomalies in the central equatorial Pacific drive a pronounced Rossby Wave train response evident in V250 that arcs over the North Pacific and North America and into the tropical Atlantic (Fig. 8e).

Tropical Pacific SST trends, on the other hand, cause a decrease in precipitation over the central equatorial Pacific and an increase farther south and over the Philippines and South China Sea; precipitation anomalies are relatively muted over the western equatorial Pacific and Indian Ocean (Fig. 8f). The opposite-signed precipitation response in the central equatorial Pacific between the Counterfactual and Trend is consistent with the contrasting polarity of the local SST anomalies (recall Figs. 1b,c). Given the opposite-signed precipitation responses, why are the associated circulation responses over the North Pacific of the same sign (recall Figs. 7e,f and k,l)? The V250 wave train response to the tropical Pacific SST trends emanates from the anomalous drying in the central equatorial Pacific (Fig. 8f). This wave train has a relatively short zonal wavelength, arcing over the North Pacific into British Columbia before turning southward over the central US and into the Caribbean. The lack of an appreciable precipitation response over the western tropical Pacific preempts a wave train response emanating from the western portion of the basin. Thus, subtle differences between the spatial patterns of tropical precipitation response explain why the Counterfactual and Trend produce a same-signed teleconnection response despite their opposite-signed SST anomalies. These differences in turn arise from the relatively weak amplitude of SST anomalies in the central equatorial Pacific in the Trend compared to the Counterfactual.

To further substantiate the dynamical pathways for the tropical Indo-Atlantic and Pacific teleconnections, we examine the RWS and WAF responses. Tropical Indo-Atlantic 2023-24 SST anomalies and SST trends induce a negative RWS anomaly centered over and to the west of Japan, directly north of the region of diminished precipitation over the western tropical Pacific (Figs. 9a,c). This RWS anomaly results from a negative anomaly in the vortex stretching term, with

contributions from both relative and planetary vorticity, which is slightly offset by a positive anomaly in the vorticity advection term (not shown). The anomalous vortex stretching is associated with northerly 250hPa divergent wind anomalies to the south that develop in response to (i.e., converge into) the region of diminished precipitation over the northwestern tropical Pacific (Figs. 9a,c). A positive RWS anomaly is found over the central North Pacific at the jet exit region; this anomaly results from the planetary vorticity stretching term (not shown) likely associated with the anomalous ridge at upper levels (recall Figs. 7d,f). The WAF anomalies triggered by the anomalous RWS approximately trace the pathway of the upper-level teleconnection pattern (Fig. 9d,f). We speculate that the reason why the Counterfactual component of tropical Indo-Atlantic SST anomalies does not drive an appreciable NH teleconnection is that the tropical precipitation response is confined to the Indian Ocean where the mean state upper-level winds are easterly, inhibiting Rossby Wave propagation (Fig. 9b; gray contour encloses regions of mean easterlies).

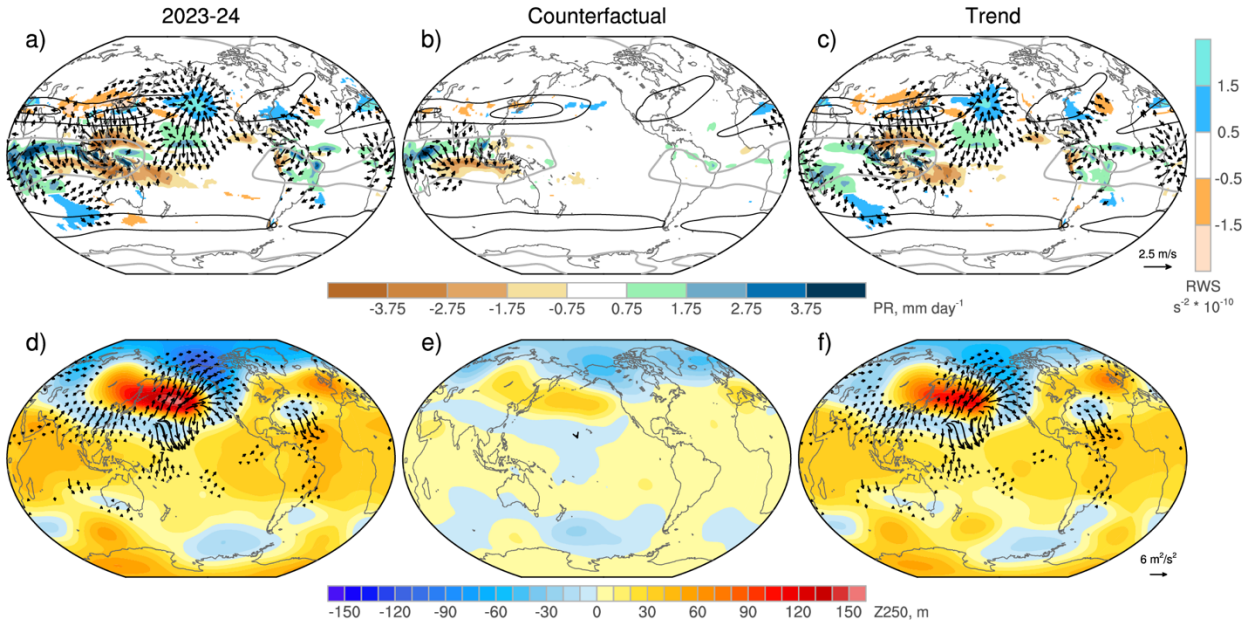

Figure 9. CAM6 DJF responses to Tropical Indo-Atlantic SST anomalies: (a,d) [TropIndAtl 2023-24] – [CTL1980]; (b,e) [TropIndAtl Counterfactual] – [CTL1980]; (c,f) [TropIndAtl 2023-24] – [TropIndAtl Counterfactual]. (Top row) Precipitation (mm d^{-1}; color shading shown in the horizontal color bar), 250 hPa divergent wind vectors (ms^{-1}; reference vector is shown in the lower right; magnitudes near zero are omitted), and RWS ($x10^{-10}$ s^{-2}; color shading shown in the vertical color bar). Contours show the climatological U250 (black for 40 and 50 ms^{-1}; gray for zero ms^{-1}). (Bottom row) Z250 (m; color shading) and WAF vectors ($x10^{-10}$ s^{-2}; reference vector shown in the

lower right; magnitudes near zero are omitted). For clarity, only precipitation values over the tropics (25°N-25°S) and RWS values over 25°-55°N and 25°-55°S are shown.

The 2023-24 and Counterfactual SST anomalies in the Tropical Pacific induce a positive RWS anomaly along the northern edge of the jet stream core, extending from eastern China to the central North Pacific (Figs. 10 a,b). This zonally-elongated RWS anomaly has two origins: east of Japan, it is associated with upper level wind anomalies diverging out of the positive precipitation anomaly in the west-central tropical Pacific (Figs. 10 a,b), which induce a positive RWS anomaly via the (primarily planetary vorticity) stretching term (not shown); west of Japan, it results from upper level wind anomalies converging into the negative precipitation anomaly over the Maritime Continent, which induces a positive RWS anomaly via the (relative) vorticity advection term (not shown). The anomalous WAF vectors over the central North Pacific emanate from the positive RWS anomaly, delineating the path of the Rossby wave train over the Pacific-North American sector (Fig. 10 d,e). Anomalous northward WAF vectors are also seen to emanate from the positive precipitation anomaly over the far eastern tropical Pacific, consistent with the signature in V250 (recall Fig. 8 d,e). The RWS anomalies induced by Tropical Pacific SST trends are much weaker than those driven by the 2023-2024 and Counterfactual SST anomalies, consistent with the weaker precipitation response in the western and central tropical Pacific (Fig. 10c). The anomalous WAF vectors are mainly located over the eastern North Pacific and trace the path of the Rossby wave train evident in V250 (Fig. 10f). The short zonal wavelength of this Rossby Wave train is consistent with the weaker climatological zonal winds on the eastern flank of the jet stream, which would reduce the zonal wavelength following Rossby Wave theory.

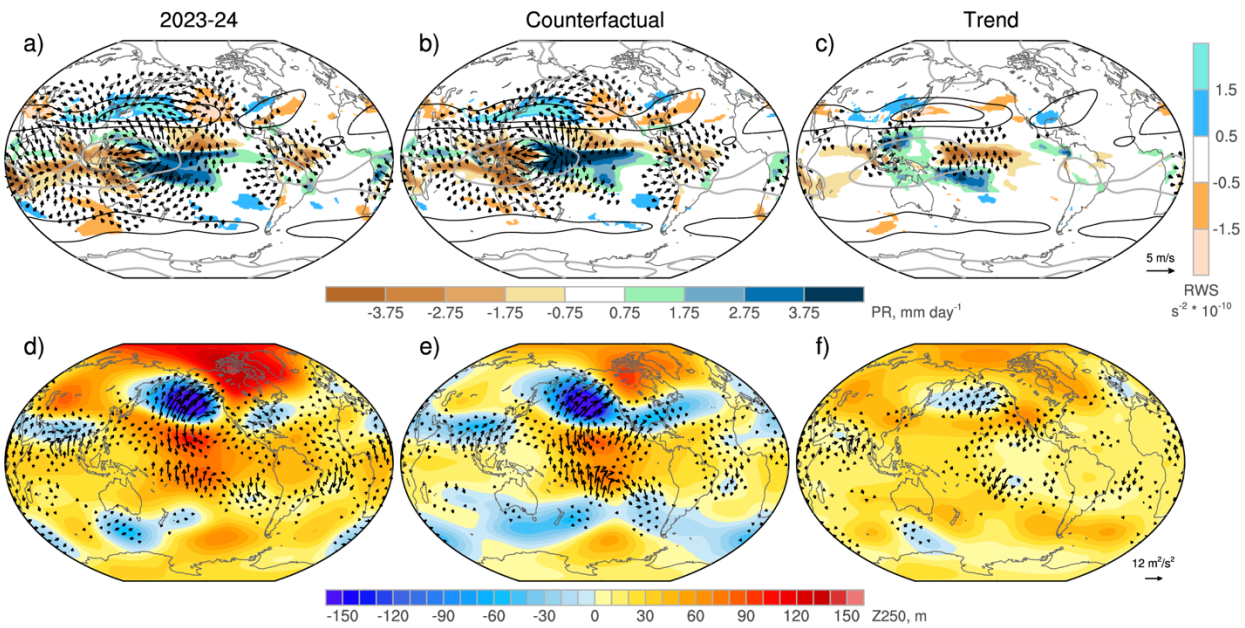

588

589 **Figure 10**. As in Fig. 9 but for Tropical Pacific SST anomalies: (a,d) [TropPac 2023-24] –
590 [CTL1980]; (b,e) [TropPac Counterfactual] – [CTL1980]; (c,f) [TropPac 2023-24] – [TropPac
591 Counterfactual]. Note the different reference vector scales compared to Fig. 9.
592
593

594 *f. Interpreting observed teleconnections during the 2023-2024 El Niño*

595 Armed with the insights gained from the CAM6 experiments, we now turn to the observations and
596 their interpretation. Just like any individual member of the CAM6 ensembles, the observed
597 circulation anomalies (especially in the extra tropics) will contain a mixture of internal atmospheric
598 variability and forced response. Thus, we do not expect a direct correspondence between the
599 observations and the CAM6 responses, since the latter, based on 50-member ensemble means,
600 isolate the forced component. Nevertheless, decomposing the observed DJF 2023-2024 SLP
601 anomalies into Counterfactual and Trend components yields results that are largely analogous to
602 the CAM6 forced responses. Like CAM6, the observed anomalies reflect offsetting influences
603 from the Counterfactual and Trend contributions, especially over the NH and tropics (Fig. 11 a-c).
604 Over the North Pacific, the Counterfactual SLP shows a pronounced negative anomaly focused in
605 the east (maximum values ~ -12hPa), while the Trend exhibits positive anomalies over much of
606 the basin (maximum values ~ 8hPa); anomalies over the Sea of Okhotsk are out-of-phase with the
607 rest of the North Pacific. Over the North Atlantic, the Counterfactual and Trend components show
608 negative and positive NAO-like patterns, respectively. Over the tropics, a negative (positive)
609 Southern Oscillation pattern is seen in the Counterfactual (Trend) component.

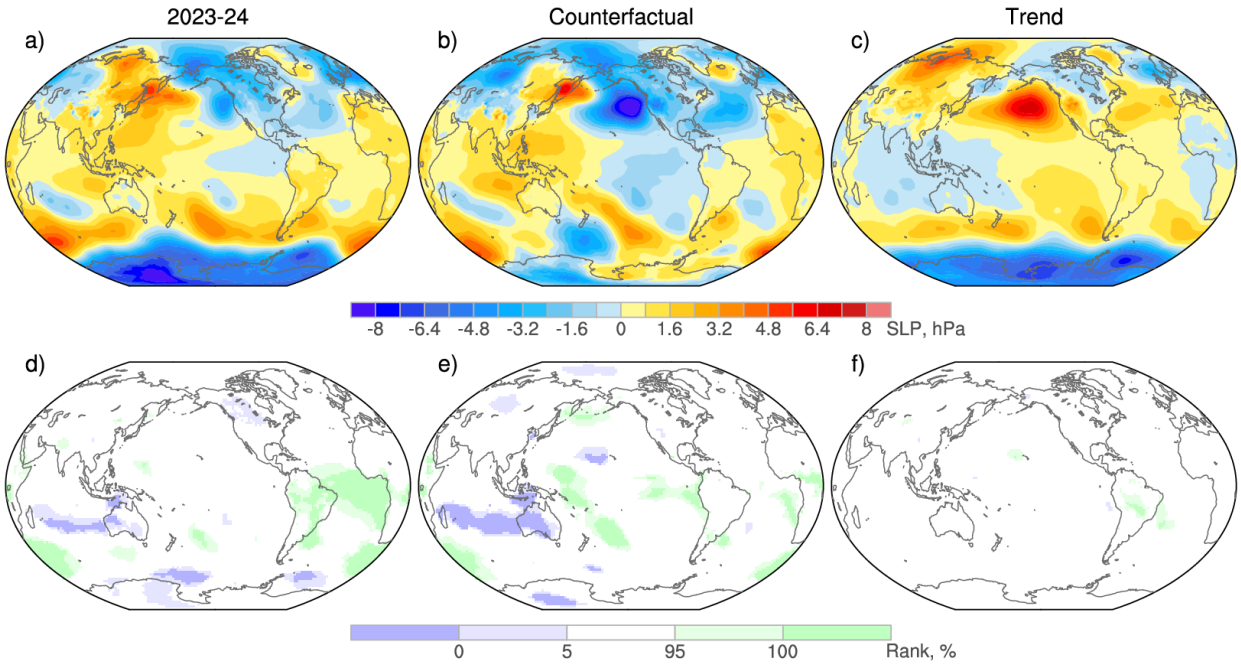

Figure 11. (a) Observed DJF 2023-2024 SLP anomalies (hPa) and their (b) Counterfactual and (c) Trend components. (d-f) Percentile rank of the observed SLP values relative to the corresponding CAM6 Global SST/SIC AMIP ensembles. White areas indicate that the observed value lies within the 5th – 95th percentile range of the CAM6 ensemble spread; dark purple (green) shading indicates that the observed value is less (greater) than the value in any individual ensemble member. For this plot, the average of [CTL1980] and [CTL2024] was subtracted from the Global SST/SIC AMIP experiments for direct comparison to observations.

While the Counterfactual and Trend contributions to observed 2023-2024 SLP anomalies are generally similar in sign to their CAM6 SST/SIC-forced counterparts (with the notable exception of the Arctic), their amplitudes and regional details differ. To assess whether this is a result of internal atmospheric variability or model bias (or possibly bias in the SST/SIC and radiative forcings), we evaluate whether the observed values lie within the CAM6 ensemble-spread. The observed 2023-2024 SLP anomalies lie within the CAM6 Global 2023-2024 AMIP ensemble spread over almost the entire NH and tropical Pacific, indicating that discrepancies between the observed anomalies and the CAM6 forced response in these areas can be attributed to internal atmospheric variability (white areas in Fig. 11d). However, the observed values lie outside the ensemble spread over the tropical Atlantic, the south tropical Indian Ocean and portions of the Southern Ocean, implicating model biases in these regions (Fig. 11d). Similarly, the observed Counterfactual values lie within the 5th – 95th percentile range of the CAM6 Global Counterfactual

ensemble-spread over most of the globe except the south tropical Indian Ocean and small areas within the tropical Pacific (Fig. 11e). The observed Trend values lie almost entirely within the CAM6 ensemble-spread (Fig. 11f).

Like the CAM6 ensemble means, observed 2023-2024 tropical precipitation shows opposite-signed anomalies between the Counterfactual and Trend components, except over the Indian Ocean where the trend contribution is small (Fig. 12 b,c). In particular, the Counterfactual anomalies reflect a northward shift of the South Pacific Convergence Zone (SPCZ) and a southward displacement of the Inter Tropical Convergence Zone (ITCZ: see Fig. A3b for the climatological precipitation distribution) along with reduced precipitation over the Maritime Continent and equatorial Atlantic, while the Trend anomalies show the opposite polarity with weaker amplitude. While the observed anomaly patterns are not reproduced in detail by CAM6 due to model bias (indicated by ranks outside of the 5^{th} – 95^{th} percentile ensemble spread; Figs. 12 g-i), the offsetting nature of the Counterfactual and Trend contributions is generally well simulated (Fig. 12 d,e). It is likely that mean state biases underpin some of the model-observation mismatches, including the climatological dry bias over the equatorial Pacific and Atlantic and south tropical Indian Ocean, and the retracted and overly zonal orientation of the SPCZ; see Fig. A3c).

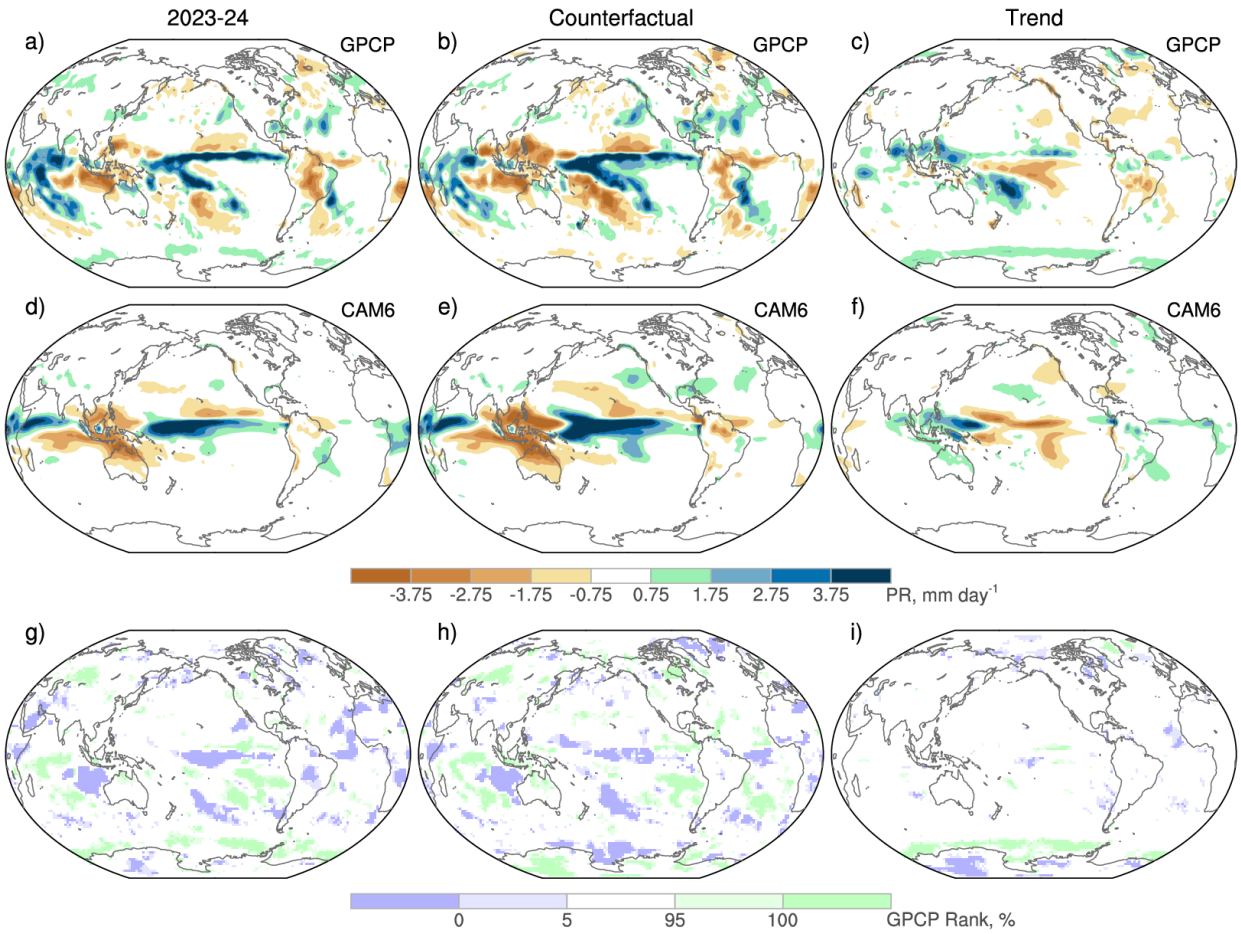

Figure 12. As in Fig. 11 but for observed precipitation from GPCP (mm day^{-1}). Middle row shows the CAM6 Global AMIP responses: d) [Global 2023-24] – [CTL1980]; (e) [Global Counterfactual] – [CTL1980]; (f). [Global 2023-24] - [Global Counterfactual]. See text for details.

Given the opposing influences of the Counterfactual and Trend components of observed NH circulation anomalies in 2023-2024, it is not surprising that observed precipitation anomalies over North America also exhibit offsetting impacts (Fig. 13 a-c). Much like the CAM6 forced responses, the Counterfactual component of observed 2023-2024 precipitation anomalies shows generally positive values over the southern US and along coastal British Columbia and Alaska, and negative values over the Ohio Valley – Upper South, parts of the upper Midwest and interior portions of western Canada and Alaska, while the Trend component shows anomalies of the opposite sign. The observed 2023-2024 precipitation anomalies over North America and their Counterfactual and Trend components lie generally within the CAM6 ensemble spreads, except for parts of central Canada and isolated pockets within the US (Figs. 13 d-f).

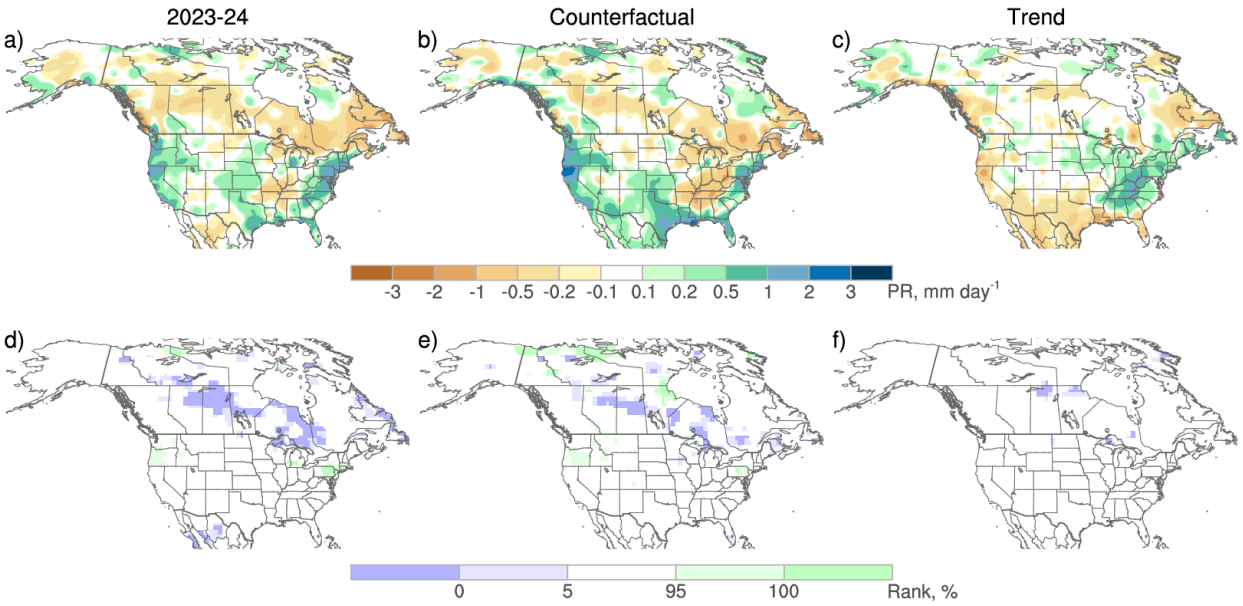

Figure 13. As in Fig. 11 but for precipitation from GPCC over North America.

Observed precipitation anomalies over Europe also exhibit analogous behavior to the CAM6 forced responses, although model biases are evident between the Adriatic and Black Seas (Fig. 14 g-l). The Counterfactual component of observed 2023-2024 precipitation shows negative anomalies over Scandinavia and southeastern Europe, with positive anomalies elsewhere, while the Trend component exhibits positive anomalies over much of Scandinavia and central Europe and negative anomalies over Germany, France, Spain and Portugal. Thus, the Counterfactual and Trend components are offsetting over northern and southern Europe, much like the CAM6 forced results although the relative balance of the two components differs somewhat. Most of the mismatches between the observed precipitation anomalies and the model responses can be attributed to internal atmospheric variability (Fig. 14 j-l), including those over Asia (Fig. A4).

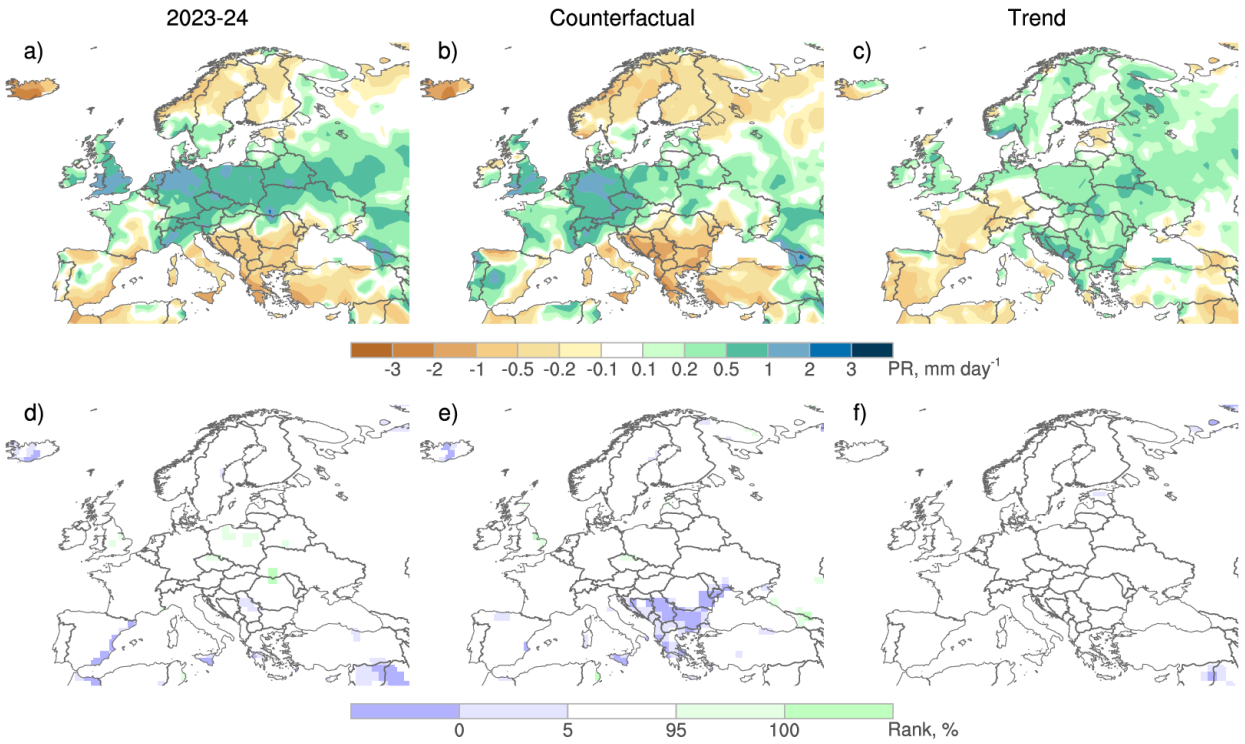

Figure 14. As in Fig. 13 but for precipitation from GPCC over Europe.

4. Summary and Discussion

The strong El Niño of 2023-2024 was unusual for its muted atmospheric circulation response, not only within the tropical Pacific (Peng et al. 2025) but extending over the entire extratropical NH (Chen et al. 2024; Zhang et al. 2025). This event occurred amidst a singular pattern of background SST trends since 1980 associated with the combined effects of global warming and natural variability. In this study, we tested the hypothesis that the background SST trend pattern was responsible for offsetting the expected El Niño teleconnection to the NH during boreal winter 2023-2024. Our results are based on a series of atmospheric general circulation experiments with CAM6 at 1° spatial resolution using observed 2023-2024 SSTs and radiative forcings, and a counterfactual version based on detrended SST anomalies and radiative forcings representative of 1979-1980. These experiments are compared against control simulations with climatological boundary conditions. A unique aspect of our experimental design is the large ensemble size (50 members) for each experiment and control simulation, which allows for a robust estimation of the forced response amidst the noise of internally generated atmospheric variability. We further elucidated the relative roles of SST anomalies *vs.* radiative forcing, tropical *vs.* extra tropical SST

anomalies, and tropical Indo-Atlantic *vs.* tropical Pacific SST anomalies in the atmospheric circulation responses to the 2023-2024 El Niño and its counterfactual and trend components. The dynamical mechanisms underlying the circulation responses were also investigated, in addition to precipitation impacts over North America and Europe. Finally, we compared the model results with the observed circulation and precipitation anomalies during 2023-2024 and their detrended counterparts, taking into account atmospheric internal variability.

Our experiments confirm the hypothesis that the expected (e.g., counterfactual) NH teleconnection to the 2023-2024 El Niño was largely counteracted by the atmospheric circulation response to the tropical SST trend pattern. This offsetting response was primarily driven by the pronounced warming trend in the tropical Indo-Atlantic, not the cooling in the central-eastern tropical Pacific, consistent with the findings of Zhang et al. (2025). In particular, tropical Indian Ocean warming likely played a dominant role by inducing a remote precipitation response (drying) over the western tropical Pacific, which in turn triggered the counteracting Rossby Wave teleconnection to the NH. This teleconnection was characterized by positive geopotential height anomalies over the North Pacific, which counteracted the canonical El Niño – induced intensification of the Aleutian Low, and positive height anomalies over the eastern North Atlantic, which partially opposed the expected negative NAO response to El Niño. The counteracting circulation patterns produced offsetting precipitation impacts over North America and Europe, leading to a muted overall response in many regions. Decomposition of the observed DJF 2023-2024 circulation and precipitation anomalies into Counterfactual and Trend components yielded results largely analogous to those of the CAM6 forced responses, taking into account the role of internal atmospheric variability. While our modeling results are consistent with previous studies on El Niño teleconnections in the absence of background SST changes (e.g., Chapman et al. 2021; Deser et al. 2017) and on the atmospheric circulation response to tropical Indian Ocean warming trends (e.g., Deser and Phillips, 2006; Hoerling et al. 2004; Hurrell et al. 2004; Hu and Federov, 2020; Hou et al. 2024), our study and that of Zhang et al. (2025) are the first to elucidate how these two influences combined to produce a weaker-than-expected response to the 2023-2024 El Niño. Understanding the role of tropical inter-basin interactions on both interannual and multi-decadal timescales would provide additional insight into the characteristics of the 2023-2024 El Niño event and its teleconnections.

Regardless of the origin of the spatial pattern of tropical SST trends since 1980, it is becoming increasingly likely that modes of natural low-frequency variability such as PDV and AMV will be superimposed upon an accelerating fingerprint of anthropogenic warming in the coming decades. The evolving contributions of natural and anthropogenic influences on background SST trend patterns will undoubtedly interfere with teleconnections driven by El Niño and La Niña events in the future. Thus, historical precedent may no longer be a reliable guide to ENSO teleconnections as anthropogenic warming patterns intensify. Crucially, if the tropical Indo-Atlantic continues to warm faster than the tropical Pacific, then El Niño teleconnections to the NH will be offset, all other factors being equal. But if the tropical SST trend pattern reverses as projected by climate models (e.g., enhanced tropical Pacific warming relative to other ocean basins), then the teleconnections will likely be exacerbated in the future, a scenario that has been emphasized in previous studies (e.g., Cai et al. 2021, Cai et al. 2023 and McGregor et al. 2022). Additional factors such as changes in amplitude and location of the SST and precipitation anomalies associated with El Niño will further modify the teleconnections in a warming world (Cai et al. 2021). Given the global societal impacts from El Niño and La Niña, additional research on the nature and predictability of the future evolution of ENSO teleconnections in a changing background climate is urgently needed.

Acknowledgements

We thank Drs. Michael Alexander, Pedro DiNezio, John Fasullo, Isla Simpson and Laurent Terray for valuable discussions during the course of this work. We also thank the three anonymous reviewers for their constructive comments and suggestions. The National Center for Atmospheric Research (NCAR) is sponsored by the NSF under Cooperative Agreement 1852977. We acknowledge high-performance computing support from the Derecho system (doi:10.5065/qx9a-pg09) provided by the NSF NCAR, sponsored by the NSF.

Data Availability Statement

All model data and analysis and visualization scripts will be made publicly available through a NCAR GLOBUS guest collection.

APPENDIX A

Sea Ice Concentration Anomalies for Model Experiments, Eurasian Precipitation Responses, and Global Precipitation Climatologies

Figure A1 shows the observed December-February (DJF) Sea Ice Concentration (SIC) anomalies (2023-24, Counterfactual and Trend) specified in the CAM6 Global AMIP experiments. Figures A2 and A4 show the DJF CAM6 precipitation responses and observed (GPCC) precipitation anomalies, respectively, over Eurasia (2023-24, Counterfactual and Trend). Figure A3 shows the DJF precipitation climatology (1979-2024) from the CAM6 2023-24 Control Experiment, observations (GPCP) and their difference.

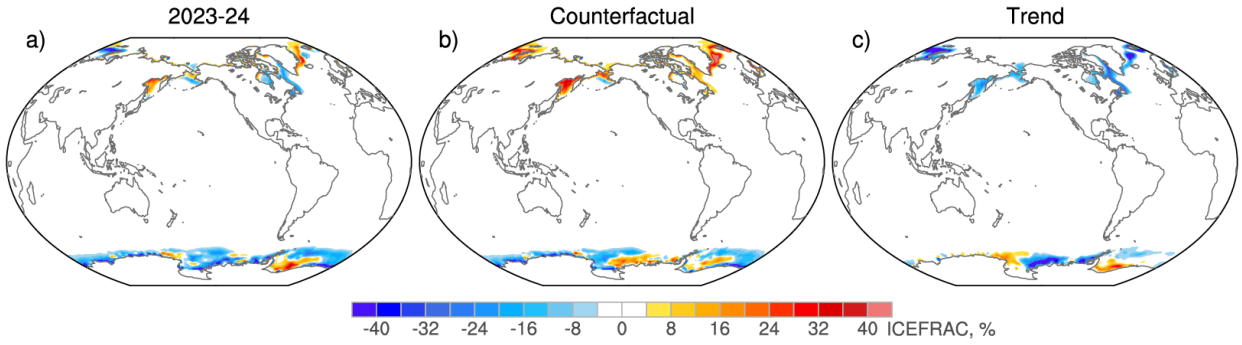

Figure A1. Observed DJF Sea Ice Concentration (ICEFRAC; %) anomalies: a) 2023-24; b) Counterfactual; c) Trend.

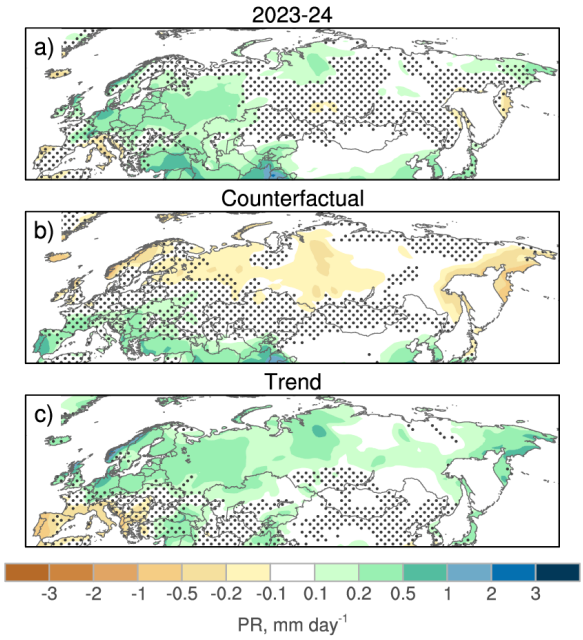

Figure A2. CAM6 DJF precipitation responses (mm day^{-1}) over Eurasia to Global SST/SIC anomalies: a) [Global 2023-24] – [CTL1980]; b) [Global Counterfactual] – [CTL1980]; c) [Global 2023-24] – [Global Counterfactual]. Responses without stippling are statistically significant at the 5% confidence level.

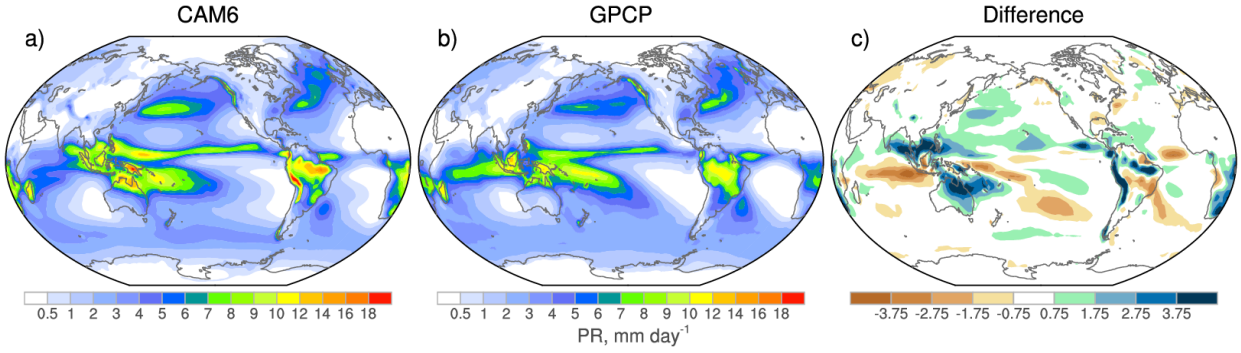

Figure A3. DJF Precipitation (PR) climatology (mm day^{-1}) based on 1979-2024: (a) CAM6 2023-24 Control Experiment; (b) GPCP; and (c) Difference (CAM6 – GPCP).

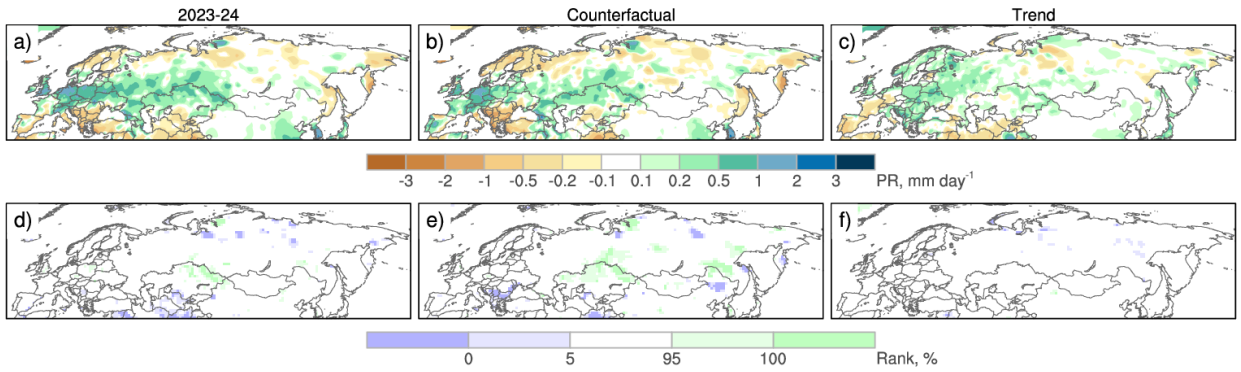

Figure A4. (a) Observed DJF 2023-2024 precipitation anomalies (mm day^{-1}) from GPCC and their (b) Counterfactual and (c) Trend components. (d-f) Percentile rank of the observed precipitation values relative to the corresponding CAM6 Global SST/SIC AMIP ensembles. White areas indicate that the observed value lies within the 5th – 95th percentile range of the CAM6 ensemble spread; dark purple (green) shading indicates that the observed value is less (greater) than the value in any individual ensemble member. For this plot, the average of [CTL1980] and [CTL2024] was subtracted from the Global SST/SIC AMIP experiments for direct comparison to observations.

References

Adler, R.F.; Sapiano, M.R.P.; Huffman, G.J.; Wang, J.-J.; Gu, G.; Bolvin, D.; Chiu, L.; Schneider, U.; Becker, A.; Nelkin, E.; et al. The Global Precipitation Climatology Project (GPCP) Monthly Analysis (New Version 2.3) and a Review of 2017 Global Precipitation. *Atmosphere* 2018, *9*, 138. https://doi.org/10.3390/atmos9040138

Alexander, M. A., I. Bladé, M. Newman, J. R. Lanzante, N. Lau, and J. D. Scott, 2002: The Atmospheric Bridge: The Influence of ENSO Teleconnections on Air–Sea Interaction over the Global Oceans. *J. Climate*, 15, 2205–2231, https://doi.org/10.1175/1520-0442(2002)015<2205:TABTIO>2.0.CO;2.

An, S.-I., Tziperman, E., Okumura, Y., & Li, T. (2020). ENSO irregularity and asymmetry. In A. Santoso, M. McPhaden & W. Cai (Eds.), El Niño Southern Oscillation in a changing climate (pp. 153–172). John Wiley & Sons.

Armour, K. C. et al., 2024: Sea-surface temperature pattern effects have slowed global warming and biased warming-based constraints on climate sensitivity, *Proc. Natl. Acad. Sci. U.S.A.* 121 (12) e2312093121, https://doi.org/10.1073/pnas.2312093121.

Barnes, E. A., and L. M. Polvani, 2013*:* Response of the midlatitude jets and of their variability to increased greenhouse gases in the CMIP5 models. *J. Climate*, *26*, 7117–7135, doi:10.1175/JCLI-D-12-00536.1.

Berner, J., H. M. Christensen, and P. D. Sardeshmukh, 2020: Does ENSO regularity increase in a warming climate? J. Climate, 33, 1247–1259, https://doi.org/10.1175/JCLI-D-19-0545.1.

Beverley, J. D., Collins, M., Lambert, F. H., & Chadwick, R. (2024). Drivers of changes to the ENSO–Europe teleconnection under future warming. *Geophysical Research Letters*, 51, e2023GL107957. https://doi.org/10.1029/2023GL107957

Beverley, J. D., M. Collins, F. H. Lambert, and R. Chadwick, 2021: Future Changes to El Niño Teleconnections over the North Pacific and North America. *J. Climate*, 34, 6191–6205, https://doi.org/10.1175/JCLI-D-20-0877.1.

Bjerknes, J., . 1969*:* Atmospheric teleconnections from the equatorial Pacific. *Mon. Wea. Rev.*, *97* , 163–172.

Cai, W. et al., 2019: Pantropical climate interactions. *Science* 363, eaav4236.

Cai, W., and Coauthors, 2021: Changing El Niño–Southern Oscillation in a warming climate. *Nat. Rev. Earth Environ*., 2, 628–644, https://doi.org/10.1038/s43017-021-00199-z.

Cai, W., Ng, B., Geng, T. et al. Anthropogenic impacts on twentieth-century ENSO variability changes. Nat Rev Earth Environ 4, 407–418 (2023). https://doi.org/10.1038/s43017-023-00427-8

Capotondi, A., and Coauthors, 2015: Understanding ENSO Diversity. *Bull. Amer. Meteor. Soc*., 96 (6), 921–938, https://doi.org/10.1175/BAMS-D-13-00117.1.

Chang, P., and Coauthors, 2006: Climate Fluctuations of Tropical Coupled Systems—The Role of Ocean Dynamics. *J. Climate*, 19, 5122–5174, https://doi.org/10.1175/JCLI3903.1.

Chapman, W. E., A. C. Subramanian, S. Xie, M. D. Sierks, F. M. Ralph, and Y. Kamae, 2021: Monthly Modulations of ENSO Teleconnections: Implications for Potential Predictability in North America. *J. Climate*, 34, 5899–5921, https://doi.org/10.1175/JCLI-D-20-0391.1.

Chen, M., Kumar, A., L'Heureux, M., Peng, P., Zhang, T., Hoerling, M. P., & Diaz, H. F. (2024). Why do DJF 2023/24 upper-level 200-hPa geopotential height forecasts look different from the expected El Niño response? *Geophys. Res. Lett*., 51, e2024GL108946. https://doi.org/10.1029/2024GL108946

Danabasoglu, G., Lamarque, J. F., Bacmeister, J., Bailey, D. A., DuVivier, A. K., Edwards, J., et al. (2020). The Community Earth System Model version 2 (CESM2). *Journal of Advances in Modeling Earth Systems*, 12. https://doi.org/10.1029/2019MS001916

Deser, C., and A. S. Phillips, 2006: Simulation of the 1976/1977 climate transition over the North Pacific: Sensitivity to tropical forcing. *J. Climate*, 19, 6170-6180.

Deser, C., and Coauthors, 2012: ENSO and Pacific Decadal Variability in the Commu nity Climate System Model Version 4. *J. Climate,* 25 (8), 2622–2651, https://doi.org/ 598 10.1175/JCLI-D-11-00301.1.

Deser, C., Simpson, I. R., McKinnon, K. A., & Phillips, A. S. (2017). The Northern Hemisphere extra-tropical atmospheric circulation response to ENSO: How well do we know it and how do we evaluate models accordingly? *Journal of Climate*, 30, 5059–5082. https://doi. org/10.1175/JCLI-D-16-0844.1

DiGirolamo, N., Parkinson, C. L., Cavalieri, D. J., Gloersen, P., & Zwally, H. J. (2022). Sea ice concentrations from nimbus-7 SMMR and DMSP SSM/I-ssmis passive microwave data Version 2 [Dataset]. NASA National Snow and Ice Data Center Distributed Active Archive Center. https://doi.org/10.5067/MPYG15WAA4WX

Dong, Y., Armour, K. C., Proistosescu, C., Andrews, T., Battisti, D. S., Forster, P. M., et al. (2021). Biased estimates of equilibrium climate sensitivity and transient climate response derived from historical CMIP6 simulations. *Geophysical Research Letters*, 48, e2021GL095778. https://doi.org/10.1029/2021GL095778

Dong, Y., Proistosescu, C., Armour, K. C. & Battisti, D. S. Attributing historical and future evolution of radiative feedbacks to regional warming patterns using a Green's function approach: the preeminence of the western Pacific. *J. Clim.* 32, 5471–5491 (2019).

Drouard, M., and C. Cassou, 2019: A modeling- and process oriented study to investigate the projected change of ENSO forced wintertime teleconnectivity in a warmer world. *J. Climate*, 32, 8047–8068, https://doi.org/10.1175/JCLI-D-18-0803.1.

Gershunov A and Barnett T P 1998 Interdecadal modulation of ENSO teleconnections *Bull. Am. Meteorol. Soc.* 79 2715–26

Harrison, D. E., and N. K. Larkin, . 1998b: Seasonal U.S. temperature and precipitation anomalies associated with El Niño: Historical results and comparison with 1997–98. *Geophys. Res. Lett*., 25 , 3959–3962.

Heede, U. K., and A. V. Fedorov, 2023: Towards understanding the robust strengthening of ENSO and more frequent extreme El Niño events in CMIP6 global warming simulations. *Climate Dyn*., 61, 3047–3060, https://doi.org/10.1007/s00382023-06856-x.

Held, I. M., S. W. Lyons, and S. Nigam, 1989*:* Transients and the extratropical response to El Niño. *J. Atmos. Sci.*, *46* , 163–174.

Hersbach, H., and Coauthors, 2020: The ERA5 global reanalysis. *Q J R Meteorol Soc*., 146 (730), 1999–2049, https://doi.org/10.1002/qj.3803.

Hoerling, M.P., Hurrell, J.W., Xu, T. *et al.* Twentieth century North Atlantic climate change. Part II: Understanding the effect of Indian Ocean warming. *Climate Dynamics* 23, 391–405 (2004). https://doi.org/10.1007/s00382-004-0433-x

Horel, J. D., and J. M. Wallace, 1981: Planetary-scale atmospheric phenomena associated with the Southern Oscillation. *Mon. Wea. Rev*., 109, 813–829, https://doi.org/10.1175/1520-0493 (1981)109,0813:PSAPAW.2.0.CO;2.

Hou, Y., Xie, SP., Johnson, N.C. *et al.* , 2024: Unveiling the Indian Ocean forcing on winter eastern warming – western cooling pattern over North America. *Nat. Commun*., 9654. https://doi.org/10.1038/s41467-024-53921-y

Hu, S., Fedorov, A.V. Indian Ocean warming as a driver of the North Atlantic warming hole. *Nat Commun* 11, 4785 (2020). https://doi.org/10.1038/s41467-020-18522-5

Huang, B., and Coauthors, 2017: Extended Reconstructed Sea Surface Temperature, Version 5 (ERSSTv5): Upgrades, Validations, and Intercomparisons. *J. Climate*, 30 (20), 8179–8205, https://doi.org/10.1175/JCLI-D-16-0836.1.

Huang, P., and S.-P. Xie, 2015: Mechanisms of change in ENSO-induced tropical Pacific rainfall variability in a warming climate. *Nat. Geosci*., 8, 922–926, https://doi.org/10.1038/ ngeo2571.

Hurrell, J. W., M. P. Hoerling, A. S. Phillips, and T. Xu (2004), Twentieth century North Atlantic climate change. part I: Assessing determinism, *Clim. Dyn.*, 23, 371–390.

Izumo, T., Vialard, J., Lengaigne, M., & Suresh, I. (2020). Relevance of relative sea surface temperature for tropical rainfall interannual variability. *Geophysical Research Letters*, 47, e2019GL086182. https://doi.org/10.1029/2019GL086182

Johnson, N. C., and S.-P. Xie, 2010*:* Changes in the sea surface temperature threshold for tropical convection. *Nat. Geosci.*, *3*, 842–845, https://doi.org/10.1038/ngeo1008.

Johnson, N. C., and Y. Kosaka, 2016*:* The impact of eastern equatorial Pacific convection on the diversity of boreal winter El Niño teleconnection patterns. *Climate Dyn.*, *47*, 3737–3765, https://doi.org/10.1007/s00382-016-3039-1.

Kim, J., B. Tian and J. Yu, 2025: Unusual and persistent easterlies restrained the 2023/24 El Niño development after a triple-dip La Niña. *npj climate and atmospheric sci*., https://doi.org/10.1038/s41612-024-00890-0.

Kessler, W. S., 2002: Is ENSO a cycle or a series of events? *Geophys. Res. Lett*., 29 (23), 633 40–1–40–4, https://doi.org/10.1029/2002GL015924.

Larkin, N. K., & Harrison, D. E. (2002). ENSO warm (El Niño) and cold (La Niña) event life cycles: Ocean surface anomaly patterns, their symmetries, asymmetries, and implications. *Journal of Climate*, 15(10), 1118–1140.

Lenssen, N., P. DiNezio, L. Goddard, C. Deser, Y. Kushnir, S. J. Mason, M. Newman, and Y. Okumura, 2024: Strong El Niño events lead to robust multi-year ENSO predictability. *Geophys. Res. Lett.*, 51, e2023GL106988, https://doi.org/10.1029/ 2023GL106988.

L'Heureux, M. L., D. S. Harnos, E. Becker, B. Brettschneider, M. Chen, N. C. Johnson, A. Kumar, and M. K. Tippett, 2024: How Well Do Seasonal Climate Anomalies Match Expected El Niño–Southern Oscillation (ENSO) Impacts?. *Bull. Amer. Meteor. Soc*., 105, E1542–E1551, https://doi.org/10.1175/BAMS-D-23-0252.1.

Maher, N., J. E. Kay and A. Capotondi, 2022: Modulation of ENSO teleconnections over North America by the Pacific decadal oscillation. *Environ. Res. Lett*.. 17 114005 doi10.1088/1748-9326/ac9327

Maher, N., and Coauthors, 2023: The future of the El Niño–Southern Oscillation: using large ensembles to illuminate time-varying responses and inter-model differences. *Earth System Dynamics*, 14 (2), 413–431, https://doi.org/10.5194/esd-14-413-2023.

McGregor, S., Cassou, C., Kosaka, Y., & Phillips, A. S. (2022). Projected ENSO teleconnection changes in CMIP6. Geophysical Research Letters, 49, e2021GL097511. https://doi.org/10.1029/2021GL097511

McPhaden, M. J., S. E. Zebiak, and M. H. Glantz, 2006: ENSO as an Integrating Concept in Earth Science. *Science*, 314 (5806), 1740–1745, https://doi.org/10.1126/science.1132588.

Molina, B., P. N. DiNezio and C. Deser, 2025: ENSO oscillatory regimes controlled by the zonal location of air-sea coupling region. *J. Climate*, submitted [pdf available at https://staff.cgd.ucar.edu/cdeser/].

Neelin, J. D., D. S. Battisti, A. C. Hirst, F.-F. Jin, Y. Wakata, T. Yamagata, and S. E. Zebiak (1998), ENSO theory, *J. Geophys. Res*., 103(C7), 14261–14290, doi:10.1029/97JC03424.

Okumura, Y. M., and C. Deser, 2010: Asymmetry in the Duration of El Niño and La Niña. *J. Climate*, 23 (21), 5826–5843, https://doi.org/10.1175/2010JCLI3592.1.

Peng, Q., S. -P. Xie, A. Miyamoto, C. Deser, P. Zhang and M. T. Luongo, 2025: Unusual growth of the 2023-24 El Niño against the odds of Indo-Atlantic warming. *Nat. Geosci.*, in press.

Ropelewski, C. F., & Halpert, M. S. (1987). Global and regional scale precipitation patterns associated with El Niño/Southern Oscillation. *Monthly Weather Review*, 115, 1606–1626.

Rugenstein, M., M. Zelinka, K. B. Karnauskas, P. Ceppi, and T. Andrews (2023), Patterns of surface warming matter for climate sensitivity, *Eos, 104,* https://doi.org/10.1029/2023EO230411.

Sardeshmukh, P. D., and B. J. Hoskins, 1988*:* The generation of global rotational flow by steady idealized tropical divergence. *J. Atmos. Sci.*, *45*, 1228–1251, https://doi.org/10.1175/1520-0469(1988)045⟨1228:TGOGRF⟩2.0.CO;2.

Schneider, U. et al., 2015: GPCC full data monthly product version 7.0 at 2.5°: Monthly land-surface precipitation from rain-gauges built on GTS-based and historic data.

Sobel AH, Nilsson J, Polvani LM (2001) The weak temperature gradient approximation and balanced tropical moisture waves. *J Atmos Sci* 58:3650–3665. doi:10.1175/1520-0469(2001)058<3650:TWTGAA>2.0.CO;2

Simpson, I. R., T. A. Shaw, and R. Seager, 2014: A Diagnosis of the Seasonally and Longitudinally Varying Midlatitude Circulation Response to Global Warming. *J. Atmos. Sci.*, 71, 2489–2515, https://doi.org/10.1175/JAS-D-13-0325.1.

Takaya, K., and H. Nakamura, 2001*:* A formulation of a phase-independent wave-activity flux for stationary and migratory quasigeostrophic eddies on a zonally varying basic flow. *J. Atmos. Sci.*, *58*, 608–627, https://doi.org/10.1175/1520-0469(2001)058⟨0608:AFOAPI⟩2.0.CO;2.

Thirumalai, K., P. N. DiNezio, Y. Okumura, J. Partin, Liu, K. Costa, and A. Jacobel, 2024: Future increase in extreme El Nino supported by past glacial changes. *Nature*, 634, 374–380, 665 https://doi.org/10.1038/s41586-024-07984-y.

Timmermann, A., and Coauthors, 2007: The Influence of a Weakening of the Atlantic Meridional Overturning Circulation on ENSO. *J. Climate*, 20, 4899-4919, https://doi.org/10.1175/JCLI4283.1.

Trenberth, K. E., G. W. Branstator, D. Karoly, A. Kumar, N-C. Lau, and C. Ropelewski, 1998*:* Progress during TOGA in understanding and modeling global teleconnections associated with tropical sea surface temperatures. *J. Geophys. Res.*, *103* , 14291–14324.

Wang, C., 2019: Three-ocean interactions and climate variability: a review and perspective. *Clim. Dyn*. 53, 5119–5136.

Wang, C., Deser, C., Yu, J.-Y., DiNezio, P., & Clement, A. (2016). El Niño-Southern Oscillation (ENSO): A review. In P. Glymn, D. Manzello, I. Enochs (Eds.), Coral Reefs of the Eastern Pacific (pp. 85–106). New York: Springer Science Publisher.

Watanabe, M., Kang, S.M., Collins, M. *et al.* Possible shift in controls of the tropical Pacific surface warming pattern. *Nature* 630, 315–324 (2024). https://doi.org/10.1038/s41586-024-07452-7

Wills, R. C. J., Y. Dong, C. Proistosecu, K. C. Armour, and D. S. Battisti, 2022: Systematic climate model biases in the large-scale patterns of recent sea-surface temperature and sea-level pressure change. *Geophys. Res. Lett*., 49 (17), e2022GL100 011, https://doi.org/10.1029/2022GL100011.

Wittenberg, A. T., 2009: Are historical records sufficient to constrain ENSO simulations? *Geophys. Res. Lett*., 36 (12), https://doi.org/10.1029/2009GL038710.

Yeager, S. G. et al., 2022: The Seasonal-to-Multiyear Large Ensemble (SMYLE) prediction system using the Community Earth System Model version 2. *Geosci. Model Dev.* 15, 6451–6493.

Zhang, L., Chen, Y., Karnauskas, K.B. *et al.* , 2025: The 2023/24 El Niño event exhibited unusually weak extratropical teleconnections. *Commun. Earth Environ.* **6**, 595. https://doi.org/10.1038/s43247-025-02584-8

Zhou, Z.-Q., S.-P. Xie, X.-T. Zheng, Q. Liu, and H. Wang, 2014: Global warming–induced changes in El Niño teleconnections over the North Pacific and North America. *J. Climate*, 27, 9050–9064, https://doi.org/10.1175/JCLI-D-14-00254.1.